Hydraulics Laboratory

Civil Engineering Department

Katholieke Universiteit Leuven

NUMERICAL SIMULATION OF TURBULENCE DAMPING IN SEDIMENT-LADEN FLOW

Part 1.
The "Siltman" test case and the concept of "saturation"

Report No. HYD/ET/99.2

August 1999

Erik A. TOORMAN

MAST - III
Marine Science and Technology Programme

A contribution to the MAST III project COSINUS

COSINUS

partially funded by the E.C., Directorate General XII under contract no. MAS3-CT97-0082.

NUMERICAL SIMULATION OF TURBULENCE DAMPING IN SEDIMENT-LADEN FLOW. **Part 1.** The "Siltman" test case and the concept of "saturation"

Abstract

This report presents the analysis of numerical data for sediment-laden fully-developed turbulent open-channel, obtained with a second order finite element solution of the hydrodynamic equations, the sediment transport equation and the standard two-equation k-ε turbulence model with buoyancy term in the k-equation.

First, a series of unsteady simulations, starting from a homogeneous suspension, have been carried out. When the sediment load is increased, a lutocline is temporarily formed. The high density gradient at this lutocline causes large damping of the turbulent kinetic energy, at which the code starts to have numerical problems because the validity conditions for the turbulence equations are violated, since the flow locally laminarizes. Methods to overcome these local low-Reynolds effects still need to be developed.

Following, steady state calculations have been carried for various sediment loads and gradually decreasing shear velocity (u_*). The results show that with decreasing u_*, the flux Richardson number (Rf) tends to homogenize over a large portion of the water column, starting around mid-depth. When this layer reaches the bottom, the (vertical) gradient of Rf changes sign (becomes negative). A further small decrease of u_* rapidly causes Rf to reach the ultimate critical value of 1 at which all turbulence production is completely destroyed by buoyancy damping: the numerical model fails from here on.

It is hypothesised that the value Rf_c, corresponding with the constant Rf layer, can be considered as another critical value beyond which saturation starts. However, as Rf_c is always exceeded near the surface (partly as a result of the employed free surface boundary conditions) without turbulence collapse, a second condition has been identified, which is the change of sign of Rf: when it becomes negative, saturation can occur (or, on a local scale, a lutocline is formed).

The condition $dRf/dy = 0$ results in a parabolic eddy viscosity profile, similar to the one for clear water, but in which the von Karman constant is replaced by $\sigma_s w_s/u_*$. Subsequently, it is demonstrated that the profiles of the model variables ρ, u_*, k and ε at the critical condition $Rf = Rf_c$ can be described by analytical functions, i.e. a Rouse profile with Rouse parameter $Z = 1$ and standard profiles where κ is replaced by $\sigma_s w_s/u_*$. These analytical results are confirmed by the numerical results. They imply that the von Karman coefficient is not a constant but indeed decreases with increasing sediment load, confirming the long known, but still disputed interpretation of experimental data.

The value of Rf_c is found to be significantly higher than the traditionally accepted empircal value of 0.15 for thermal or salinity stratification. It is hypothesised that the difference may be caused by the additional settling sink term in the sediment mass balance equation. The value is found to depend only on the settling velocity. Experimental evidence still need to be found.

The results are critically evaluated in terms of limitations of the model, which contains several simplifications which are not realistic (such as a constant Schmidt number).

A contribution to Task C, "Dynamics of concentrated benthic suspensions", and Task E.2, "Schematic testcases", of the MAST III COSINUS project, partially funded by the E.C., Directorate General XII under contract no. MAS3-CT97-0082.

1. INTRODUCTION

This report presents results of the 1-dimensional-vertical (1DV) simulation of sediment-laden turbulent open-channel flow. First, the time evolution of an initially homogeneous suspension in turbulent shear flow is calculated (the “Siltman” test case). Secondly, steady state calculations have been carried out for a wider variety of parameter values. The results lead to a discussion on the concept of "saturation" and the conditions for turbulence collapse in sediment-laden turbulent shear flow.

The presented results have been obtained with the finite element code FENST-2D (2nd order in space, 2-dimensional), developed by the author[1].

This report is a contribution to Task C, "Dynamics of concentrated benthic suspensions" of the MAST III COSINUS project. The “Siltman” test case was selected for the purpose of model intercomparison within the framework of Task E.2, "Schematic test cases",

2. THE CONCEPT OF "SATURATION"

The concept of "saturation" originates from the observation that under certain conditions concentration profiles in shear flows of suspensions can rapidly vary from a relatively weakly stratified to a strongly stratified condition, where a large concentration peak is formed at the bottom. Because of the large concentration gradient turbulence is damped due to the buoyancy effect. The saturation point indicates the condition when turbulence collapse occurs.

Remark: The same term is used in a different way by *Cellino & Graf* (1999) as a synonym for "capacity" condition, to indicate the point at which sediment particles start to form a deposit on the bed. This can happen before turbulence collapse occurs. Therefore, the two definitions are not equivalent.

2.1. Stability in stratified flows

Stratification is often characterized by a Richardson number. The flux Richardson number *Rf* is defined as minus the ratio of buoyancy induced damping (*G*) to shear induced production (*P*) of turbulent kinetic energy (TKE) *k*, which in 1D shear flow reduces to:

$$Rf = -\frac{G}{P} = \frac{-\frac{g}{\sigma_s}\frac{\partial \rho}{\partial y}}{\rho\left(\frac{\partial u}{\partial y}\right)^2} = \frac{-\frac{g}{\sigma_s}\frac{\Delta\rho_s}{\rho_s}\frac{\partial C}{\partial y}}{\rho\left(\frac{\partial u}{\partial y}\right)^2} \qquad \textbf{(1)}$$

where: g = gravity constant, ρ = bulk density of the suspension, C = concentration by mass, σ_s = Schmidt number, u = mean horizontal velocity, y = vertical co-ordinate, ρ_s = sediment density, $\Delta\rho_s = \rho_s - \rho_w$ (with ρ_w the density of water).

In the literature, several critical values of *Rf* are reported at which there is transition from stable (or laminar) to unstable (or turbulent) flow and vice versa. It is useful to briefly

[1] A brief description of the code can be found on the Internet at the URL:
http://sun-hydr-01.bwk.kuleuven.ac.be/hydraulics/EToorman/fenst2d.html

review the conditions for these values.

Limits for stable flow can be found by perturbation analysis. Application to inviscid stratified shear flows was pioneered by *Taylor* (1931) and *Goldstein* (1931). This is one of the few cases which can yield analytical solutions; see e.g. *Drazin & Howard* (1966) for a review. This analysis shows that 1D inviscid stratified shear flow remains stable as long as $Rf > 0.25$ (*Miles*, 1961; *Howard*, 1961). The critical value of 0.25 corresponds to the onset of instabilities at the interface (internal waves) of two fluids with different density. This is the condition for the Helmholtz-Kelvin instability.

Ludman (1967) presented a simple and elegant argument leading to the same critical value. In the case of a linear variation of the velocity and the density the stability condition can also be retrieved from the fact that, in order to generate instability, the work that must be done to effect the interchange of mass against the acceleration of gravity, per unit volume, must be larger that the kinetic energy which is available to do this work (*Chandrasekhar*, 1961):

$$\frac{1}{4}\rho\,(\delta u)^2 \;<\; -g\,\delta\rho\,\delta z \qquad \textbf{(2)}$$

or, equivalently:

$$\left(\frac{\mathrm{d}u}{\mathrm{d}z}\right)^2 \;<\; -4\,\frac{g}{\rho}\,\frac{\mathrm{d}\rho}{\mathrm{d}z} \qquad \textbf{(3)}$$

Businger (1969) shows that with different assumptions, a similar criterion can be derived which leads to $Rf_c = 1$, which is Richardson's original criterion (*Richardson*, 1920 & 1925). He concludes that energy for turbulence will be available as long as $Rf < 1$. This corresponds with the equation which describes conservation of turbulent kinetic energy k:

$$\frac{\mathrm{d}k}{\mathrm{d}t} \;=\; \frac{\partial}{\partial y}\left(\left(\nu + \nu_t\right)\frac{\partial k}{\partial y}\right) + P + G - \varepsilon \qquad \textbf{(4)}$$

where: ν = kinematic viscosity of the suspension, ν_t = eddy viscosity, ε = dissipation rate . Since $P + G = P\,(1 - Rf)$, turbulence *can* be generated as long as $Rf < 1$.

Note that there are also conditions under which the flow remains stable at lower values of Rf. Previous condition is a necessary, but not a sufficient condition for instability. Mixing over the interface thus *can* occur for $Rf < 0.25$. The case of viscous stratified fluids is much more complex (*Drazin*, 1962).

Recent direct numerical simulation (DNS) results by *Jacobitz et al.* (1997) yield critical Richardson numbers in the range $0.06 < Rf_c < 0.24$, with a strong dependence on the Taylor scale Reynolds number (Re_λ) and the shear number ($= k\,\varepsilon^{-1}\mathrm{d}u/\mathrm{d}y$). *Werne & Fritts* (1999) also found for their DNS simulation of Kelvin-Helmholtz instability that Rf remained smaller than 0.25.

Assuming that the same limits apply to the reverse problem of stabilization or turbulence collapse, is not evident. It is very likely that there is some sort of hysteresis. Experimental data (mainly in thermal or salt stratified flow) suggest complete damping of turbulence for a critical gradient Richardson number Ri_c of the order of 0.1 or smaller (*Turner*, 1973), corresponding to a flux Richardson number of $Rf_c = Ri_c/\sigma_s \approx 0.15$ (assuming $\sigma_s = 0.7$ as in neutral conditions). Some data, however, e.g. as shown in *Turner* (1973) (fig.1), indicate the possibility of higher values (0.3 and even higher). *Werne & Fritts* (1999) admit that "some measurements suggest that turbulence, once initiated, persists for Rf significantly greater than 0.25, supporting the concept of `Richardson number hysteresis' (*Stull*, 1988)".

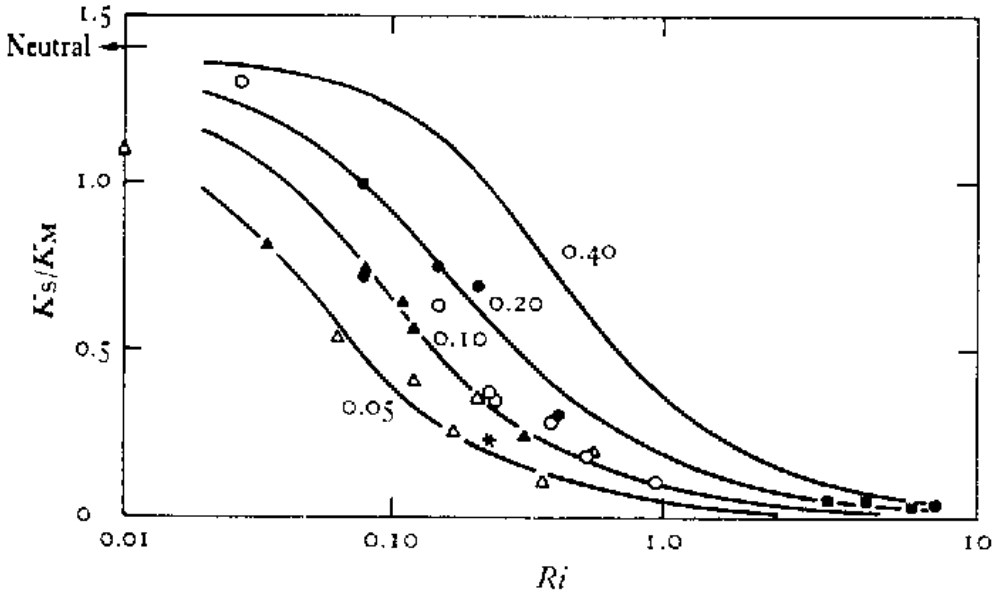


Figure 1: Ratio of transport coefficients for salt and momentum ($K_M = \nu_t$ and $K_S/K_M = 1/\sigma_s$), i.e. the inverse Schmidt number, as a function of the gradient Richardson number. Symbols = experimental data; lines = theory of *Ellison* (1957) for different values of Ri_c (figure 5.13 from *Turner*, 1973).

2.2. Saturation concentration

Using the critical value for turbulence collapse, a local condition for saturation was derived by *Teisson et al.* (1992) as follows. Assuming equilibrium, the local concentration is given by the sediment mass balance equation as:

$$C = \frac{\nu_t}{\sigma_s w_s}\left(-\frac{\partial C}{\partial y}\right) \qquad \textbf{(5)}$$

where: w_s = settling velocity. Eliminating the concentration gradient with the help of eq.(1) yields:

$$C = \rho\,\nu_t \left(\frac{\partial u}{\partial y}\right)^2 \frac{Rf}{g w_s \Delta\rho_s/\rho_s} \qquad \textbf{(6)}$$

The horizontal momentum in the case of fully-developed open-channel flow (equilibrium) can be integrated over y to yield:

$$\tau(y) = \rho\,(\nu + \nu_t)\frac{\partial u}{\partial y} = p'(h-y) \qquad \textbf{(7)}$$

where: h = water depth, $p' = \mathrm{d}p/\mathrm{d}x$, the horizontal pressure gradient, which is constant with depth and has the value $p' = \rho u_*^2/h$. Substitution, neglecting ν, yields:

$$C = \frac{\rho u_*^2}{g w_s \Delta\rho_s/\rho_s}\, Rf\, \frac{\partial u}{\partial y}(1 - y/h) \qquad \textbf{(8)}$$

Hence:

$$C = \frac{\frac{\rho_w u_*^2}{g w_s \Delta\rho_s/\rho_s} Rf \frac{\partial u}{\partial y}(1 - y/h)}{1 - \frac{u_*^2}{g w_s} Rf \frac{\partial u}{\partial y}(1 - y/h)} \qquad \textbf{(9)}$$

Substitution of the critical value may give a *local* critical "saturation" concentration at which turbulence is expected to collapse. Assuming $C \ll \rho \approx \rho_w$ and a logarithmic velocity profile, i.e. $\partial u/\partial y = u_*/\kappa y$, one can simplify previous expression to (*Teisson et al.*, 1993):

$$C_{sat} = \frac{\rho_w u_*^3 Rf_c}{\kappa y g w_s \Delta\rho_s/\rho_s}(1 - y/h) \qquad \textbf{(10)}$$

Winterwerp (1999) proposes to integrate this relationship in order to calculate the total amount of sediment which can be held in suspension. Physically, this does not seem to make much sense, as eq.(10) does not describe a concentration profile, since *Rf* in general is not constant over the water column. Furthermore, as eq.(10) yields an infinite value for $y = 0$, it can only be integrated down to a certain small distance δ away from the bottom (as for Rouse profiles). The numerical results of *Winterwerp* (1999) indicate that the depth-averaged "saturation" concentration is proportional to $U^3/w_s h$, were U = depth-averaged flow velocity (not u_* !).

2.3. Conditions for turbulence collapse

There are indications that the Richardson number alone does not suffice to explain "saturation". Consider the *Rf* profiles obtained for test case 1 (fig.2.6). They show that near the surface the value of *Rf* exceeds the critical value of $Rf_c = 0.15$, without any effect of damping or lutocline formation. Hence, it seems that turbulent mixing can occur at higher values of *Rf*, even much larger than the critical value (the reason that *Rf* tends to very large values at the free surface is the fact that the boundary conditions impose a zero gradient of the velocity. Hence, in theory *Rf* at $z = h$ tends to infinity, because *Rf* is proportional to the ratio of the concentration gradient to the velocity gradient squared)[2]. This indicates that the critical flux Richardson number is not a sufficient condition to obtain "saturation".

The following argument may provide some explanation for the possibility of turbulence generation at high *Rf*. Consider the equilibrium condition for the conservation of turbulent kinetic energy k, eq.(4) with $dk/dt = 0$. In general the total net production ($P + G$) is approximately balanced by the dissipation (ε) and the diffusion is very small over most of the water column. The diffusion (D) can be split into two terms:

$$D = \frac{\partial}{\partial y}\left(\nu_t \frac{\partial k}{\partial y}\right) = \frac{\partial \nu_t}{\partial y}\frac{\partial k}{\partial y} + \nu_t \frac{\partial^2 k}{\partial y^2} \qquad \textbf{(11)}$$

[2] However, one must bear in mind that the large values are obtained as the result of a mathematical model near the surface where the boundary conditions are not well established (in particular for the k-ε model) and are not representative for reality, where 3D effects (secondary currents) always play a role.

The gradient of k generally is negative and shows small variations over most of the water column (except near the boundaries; e.g. fig.5.5). The second term is positive and much smaller than the first over most of the column (except near the surface and the bottom) and does not need to be considered. Hence, as long as the gradient of the eddy viscosity is negative (i.e. in the upper part of the water column), the diffusion is positive and stabilizes the k-equation, i.e. turbulent flow can exist independent on the value of the Richardson number. In the layer near the bottom, where $\partial \nu_t / \partial y > 0$, however, the diffusion is negative and destabilizes, i.e. turbulence can be suppressed and collapse is possible. This explanation will be evaluated in section 4.6.

Numerical experiments, discussed in the following sections, will be analysed in view of getting a further understanding of the conditions for turbulence collapse in sediment-laden flows.

3. THE "SILTMAN" TEST CASE

3.1. Test case description

The "Siltman" test case is named after the original project in which context similar numerical tests were carried out at Delft Hydraulics (*Winterwerp*, 1998).

The test case considers the evolution in time of fully-developed turbulent open-channel flow of an initially homogenous suspension. This implies that the particles are considered non-buoyant ($w_s = 0$) at time $t \leq 0$ and buoyant ($w_s > 0$) at $t > 0$. Hence, the initial conditions are artificial. Nevertheless, this test case has proven to be interesting because of the temporary formation of lutoclines which causes much damping by buoyancy effects and poses some big challenges to the numerical code.

For the intercomparison of various models used within the framework of Task E.2 of the MAST3 COSINUS project, it has been proposed to test two conditions, i.e. were the initial concentration C_0 equals 0.010 and 0.023 g/l respectively. The other parameters are:

h	= water depth	= 16 m
U	= depth-averaged flow velocity	= 0.2 m/s
w_s	= settling velocity	= 0.5 mm/s
y_0	= roughness parameter	= 0.1 mm
ρ	= water density	= 1020 kg/m^3
μ	= water viscosity	= 1.4 10^{-3} Pa.s
σ_s	= Schmidt number	= 0.7
κ	= von Karman constant	= 0.41

Remark: The roughness parameter is related to a physical roughness height k_s by the empirical relationship $y_0 = k_s/30$ (e.g. *Booij*. 1992).

3.2. Mesh

The 1DV problem is solved on a 2D grid of one column of elements. In order to compare with the DELFT-1P model, the same mesh should be employed, i.e. a regular mesh consisting of 101 equally-spaced nodes (100 layers).

However, the bottom mesh may need some attention, depending on the used numerical method. In the case of the finite element code FENST with the standard high-*Re* turbulence model module, the law-of-the-wall is used and the first mesh node is taken some distance δ from the wall. Theoretically, this distance should lie in the range $60 < \delta_+ = \delta u_*/\nu < 120$ in order to fulfil the conditions for which the standard boundary conditions are approximately (!) valid. The code FENST has been adapted to extend this range to larger wall distances by including the pressure gradient contribution in the calculation of the shear velocity.

The highest concentration peak generally is found at the bottom. As the traditional k-ε model cannot integrate up to the bottom, the sediment in the bottom layer cannot be accounted for, unless exchange (deposition and entrainment) is allowed and the amount of sediment in the bottom layer continuously memorized. The choice of the near-bottom node of the computational mesh is thus important and should preferably be as close as possible to the bottom.

Unfortunately, natural sediment beds are not flat and bottom roughness complicates the definition of the bottom.

3.3. Bottom roughness

The given roughness $y_0 = 0.001$ m corresponds to a physical roughness height of $k_s = 30y_0 = 0.03$ m. In order to be safely out of the viscous sublayer, the first grid point should be taken at a distance of approximately $y_+ = 100$, i.e. $y_{min} = 100\ \nu/u_* = 100\ 10^{-6}/0.00945 = 0.0106$ m. Consequently, roughness elements enter the turbulent layer. This creates a problem of defining the bottom, which has important consequences.

In practice, the thickness of the viscous sublayer around the roughness elements is assumed to be small enough to be negligible. It remains difficult to make a proper choice of the near-bottom node with regard to accounting for the sediment in the bottom layer. For the "Siltman" test case, all the sediment is kept within the computational domain. Consequently, the choice of the near-bottom node will affect the solution. In order to approach the physical state, it seems recommended to choose the near-bottom node somewhere in the range $y_{min} < \delta < k_s$. In this way, at least some sediment in between the roughness elements is accounted for.

Two values of δ have been investigated: $\delta = 0.02$ m (corresponding to $\delta_+ = 130$), which is approximately the average of y_{min} and k_s, and $\delta = 0.08$ m, which is the distance from the wall where boundary conditions for k and ε are defined in the simulations by *Winterwerp*. The closer one approaches the wall, the more refinement is needed in order to capture the large gradients and to obtain a good enough value of the shear velocity (which comparison with the theoretical value for a steady state test case is a useful check on the performance of the code). The presented results for the unsteady state calculations in this section have been obtained with a wall distance of 0.08 m. An intercomparison between results for the two values in steady state calculations is given in Section 4.

3.4. Start profiles

For the results obtained with FENST-2D, presented in this report, start profiles for velocity, k and ε are obtained from a steady state calculation of the homogeneous suspension considered as non-buoyant (i.e. $w_s = 0$ mm/s).

Contrary to the procedure employed at the KUL, the start profiles used by *Winterwerp* are analytical approximations. The initial velocity profile is approximated by a power law:

$$u(0,y) = a\, y^{b} \qquad \textbf{(12)}$$

with: $a = 0.1546$ and $b = 0.14$. The initial TKE (k) profile is given by:

$$k(0,y) = \frac{u_*^2}{\sqrt{c_\mu}} \left(1 - y/Y\right) \qquad \textbf{(13)}$$

with: $Y = 23$. The initial TDR (ε) profile is given by the asymptotic behaviour:

$$\varepsilon(0,y) = u_*^3/\kappa y \qquad \textbf{(14)}$$

Another option (employed e.g. at LNH) would be to assume a linear stress profile and validity of the log-law, which results in the ideal parabolic eddy viscosity profile:

$$\nu_t = \kappa\, u_* y \left(1 - y/h\right) \qquad \textbf{(15)}$$

3.5. Determination of the initial shear velocity and pressure gradient

The velocity distribution according the log-law reads:

$$u = \frac{u_*}{\kappa} \ln(y/y_0) \tag{16}$$

The depth-average velocity is obtained as:

$$\bar{u} = \frac{1}{h}\int_{y_0}^{h} u \, \mathrm{d}y = \frac{u_*}{\kappa h}\left[y \ln\frac{y}{y_0} - y \right]_{y_0}^{h} = \frac{u_*}{\kappa}\left(\ln\frac{h}{y_0} - 1 + \frac{y_0}{h} \right) \tag{17}$$

For a given average velocity of 0.2 m/s, $y_0 = 1$ mm and $h = 16$ m, one finds a shear velocity of $u_* = 0.009447$ m/s. The corresponding wall shear stress $\rho u_*^2 = 0.09104$ Pa and the pressure gradient $\rho u_*^2/h = 0.005654$ Pa/m.

3.6. Updating the pressure gradient

The pressure is imposed upstream and downstream of the grid column as a natural boundary condition and the corresponding pressure gradient provides the required forcing. The pressure gradient is updated at each time step in order to keep the depth-averaged velocity (approximately) constant. This is done as follows (*Winterwerp*, 1998):

$$\frac{\mathrm{d}p}{\mathrm{d}x} = \rho\left(\frac{u_*^2}{h} + \frac{U_0 - U}{2\Delta t} \right) \tag{18}$$

where: Δt = the time step. This equation is obtained from the depth-integrated x-momentum equation with relaxation added.

3.7. Bottom boundary conditions

For the momentum equation, the DELFT model imposes the bottom shear stress. In FENST the bottom velocity is calculated iteratively using the law-of-the-wall.

For the sediment, the bottom flux is set zero. This implies that all the sediment is kept within the computational domain. For the present finite element implementation this implies that no sediment is allowed in the wall layer, which is outside this domain. Consequently, the simulated situation is physically incorrect. In order to take the bottom layer into account, one should use a low-*Re* formulation. However, damping functions for sediment-laden flows are not yet available.

For the k-ε model the traditional assumption of equilibrium between production and dissipation is generalized to include the buoyancy term, i.e. the bottom boundary condition for ε becomes:

$$\varepsilon(y=0) = \frac{u_*^3}{\kappa y}\sqrt{1 - Ri_f} \tag{19}$$

It is found that this correction only is important when the bottom concentration gradient becomes large. One could also raise the question whether the other assumptions (i.e. constant $k = u_*^2/c_\mu^{1/2}$, $\varepsilon = P + G$, log-law, constant κ) are still valid when there is important stratification at the bottom.

3.8. Surface boundary conditions

Best results (least convergence problems due to lutocline formation) are obtained with the Hossain-Rodi free surface conditions for k and ε (*Rodi*, 1980), because the eddy viscosity retains a finite value at the surface.

For the Navier-Stokes equation the surface traction is set zero, which in the present 1D case is equivalent to imposing a zero vertical velocity gradient. For the sediment transport equation a zero flux is imposed, i.e. the settling flux is balanced by the diffusive flux.

3.9. Results

Case 1: $C_0 = 0.010$ g/l

Time step $\Delta t = 60$ seconds; $\delta = 0.08$ m. The calculated profiles of velocity, concentration, k, ε, eddy viscosity and flux Richardson number are shown in Figures 2.1-2.6. Steady state is reached within a time span of about 10 hours. The final concentration profile differs from the theoretical Rousian profile because of the buoyancy effect, which is neglected in the theory of Rouse. There are no numerical problems with this case.

Remark: The initial velocity profile has a slightly higher average velocity, as it is the steady state result corresponding to the theoretically deduced pressure gradient.

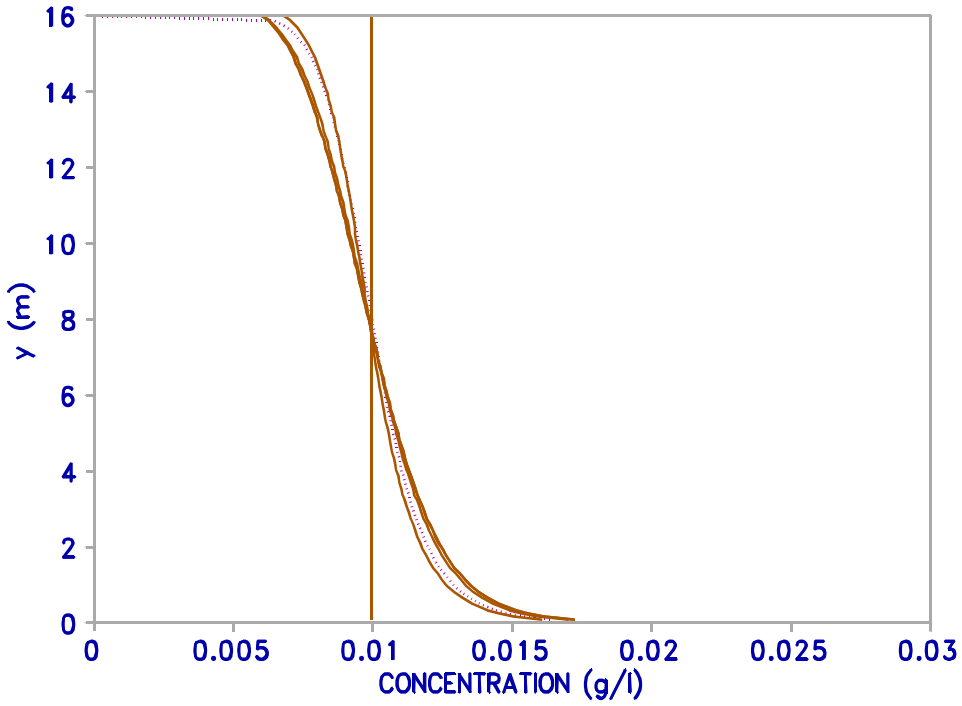


Figure 2.1: Concentration profiles. Dashed line = theoretical Rouse profile for the actual value of the Rouse parameter $Z = \sigma_s w_s / \kappa u_*$.

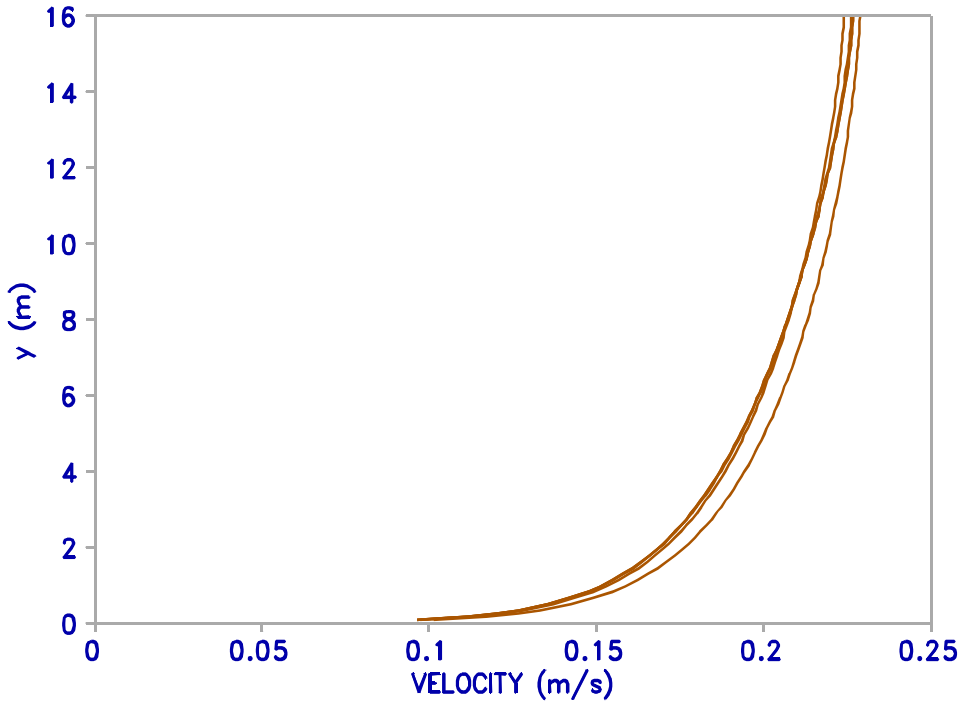


Figure 2.2: Velocity profiles.

C_0 = 10 g/l. Results at time t = 0, 100, 200, 300 and 600 minutes.

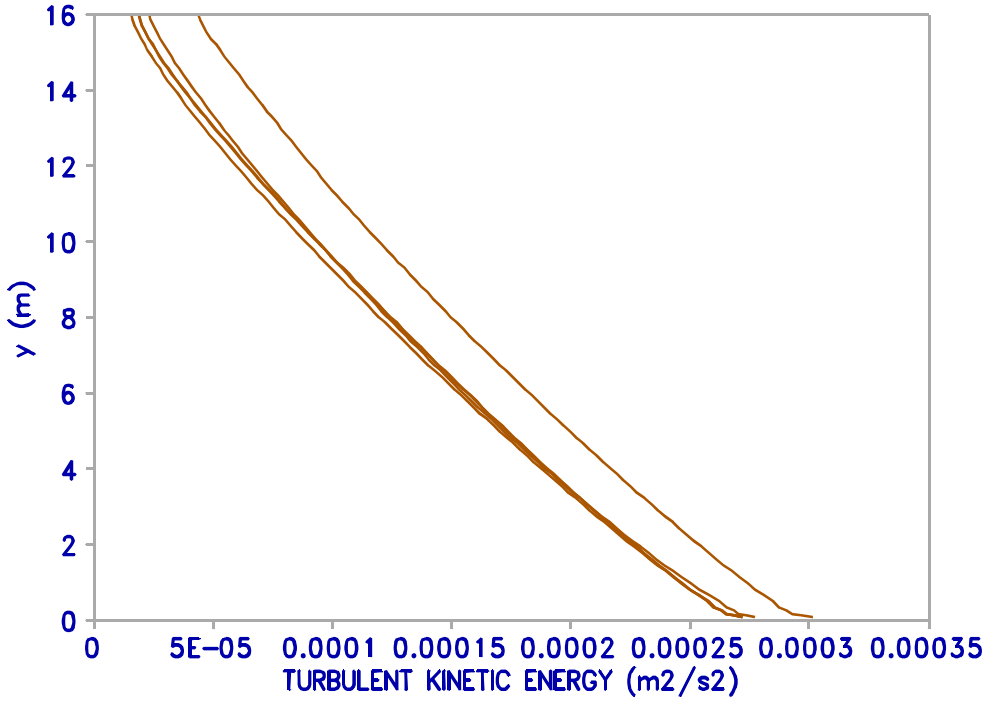


Figure 2.3: Turbulent kinetic energy (k) profiles.

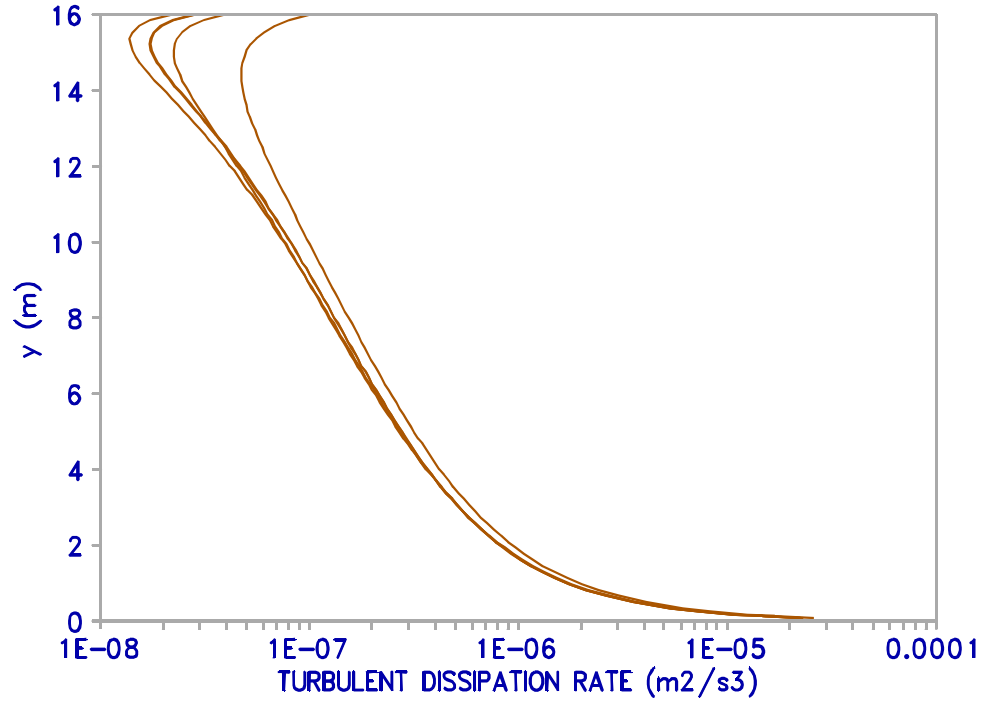


Figure 2.4: Turbulent energy dissipation rate (ε) profiles.

C_0 = 10 g/l. Results at time t = 0, 100, 200, 300 and 600 minutes.

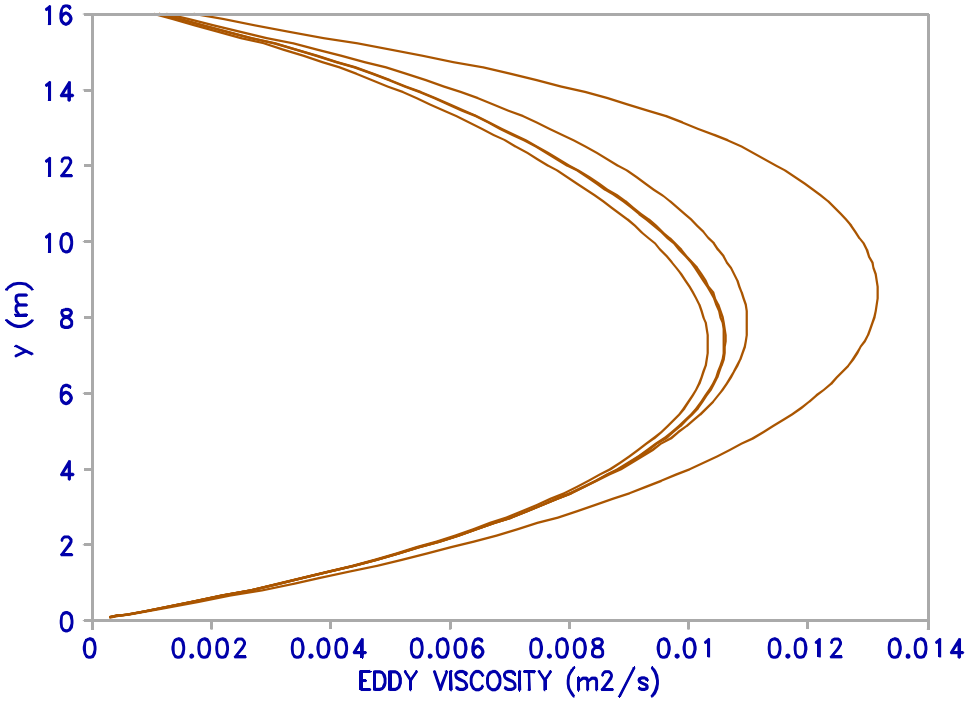


Figure 2.5: Eddy viscosity ($\nu_t = c_\mu k^2/\varepsilon$) profiles.

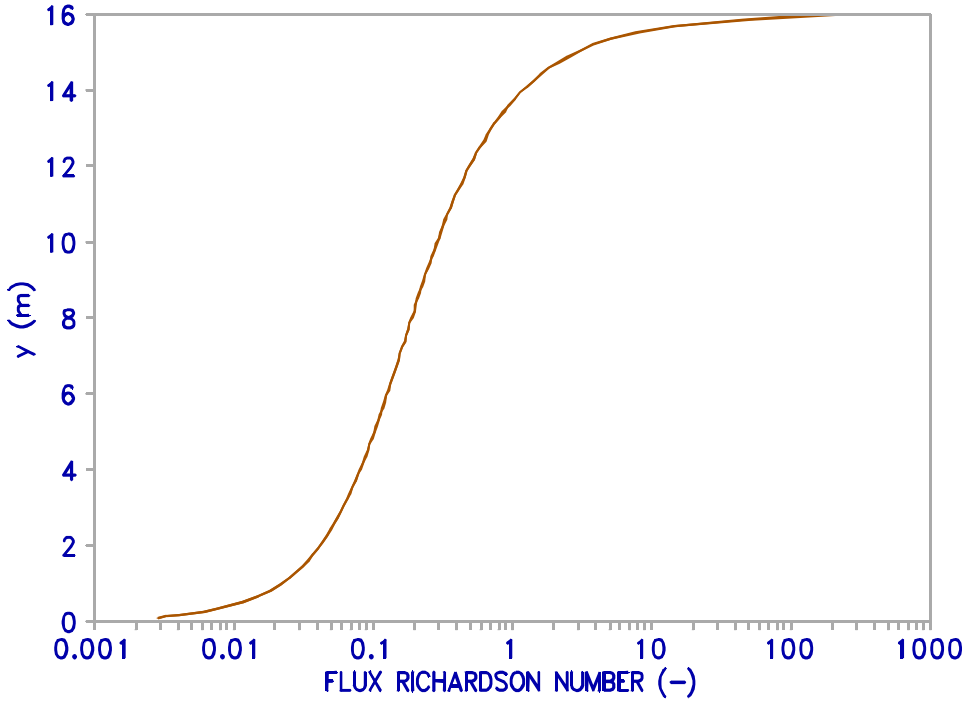


Figure 2.6: Flux Richardson number (*Rf*) profiles.

C_0 = 10 g/l. Results at time t = 0, 100, 200, 300 and 600 minutes.

Case 2: C_0 = 0.023 g/l

From preliminary numerical tests it was known that in this case a lutocline is formed and severe damping of turbulence occurs in this layer, causing serious numerical problems (*Toorman*, 1998).

In order to be able to simulate a time span of over 100 minutes, it was necessary to use a "dynamic time stepping" procedure, which means that the time step is automatically increased or decreased depending on the convergence behaviour. Calculation with a constant time step created problems due to the undershoots generated at locations with large gradients, causing negative values of C, k and/or ε.

Furthermore, it was necessary to introduce upwinding (a stabilization method for advection dominated phenomena) in the sediment transport equation to reduce undershoots in the concentration profile around the lutocline. A simplified streamline-upwind/Petrov-Galerkin (SUPG) scheme, described in (*Toorman*, 1999), has been employed. In order to reduce undershoots for the turbulence variables, it was necessary to introduce "local artificial diffusion" (LAD), which consists of adding a diffusion of the form:

$$LAD = \frac{D_{LAD}}{|\varepsilon|} \qquad \textbf{(20)}$$

to the diffusion coefficient in both the k and the ε equation (with D_{LAD} a constant). This LAD will introduce only significant diffusion when ε is small (i.e. in the nodes where turbulence is damped).

Without dynamic time stepping (DTS), calculations failed after 38 minutes. With DTS, calculations could be continued until a simulated time of $\pm$130 minutes. Results after 50 and 100 minutes are presented in Figures 3.1-3.8.

With additional artificial diffusion and truncation of the minimal values of k and ε, it was possible to run a similar case (C_0 = 24 mg/l) up to approximate steady state conditions (*Toorman*, 1998). There is another difference with the previous run: not the mean velocity, but the pressure gradient has been held constant. The results are reproduced in figure 4. Convergence problems were encountered at some time steps due to the extremely small values of k and ε (resulting in some oscillations visible on the log-scaled plots), but despite this, the calculation was continued. The values of k and ε at the lutocline are much smaller than the values obtained by the DELFT-1P model. The lutocline dissappears after some time and the final concentration profile shows that no saturation is reached.

Alternative cases

In order to reduce or even avoid the problems generated by the temporary lutocline formation, initial profiles were taken based on a previous calculation with a lower C_0. Consequently, the initial concentration profile already shows stratification. These starting conditions allowed to run simulations for higher C_0 values. Numerical simulations have been carried out for values of C_0 up to 30 mg/l without reaching saturation. This seemed to indicate that the "saturation" concentration is higher than obtained by *Winterwerp*. For higher values of C_0, problems due to lutocline formation reappeared.

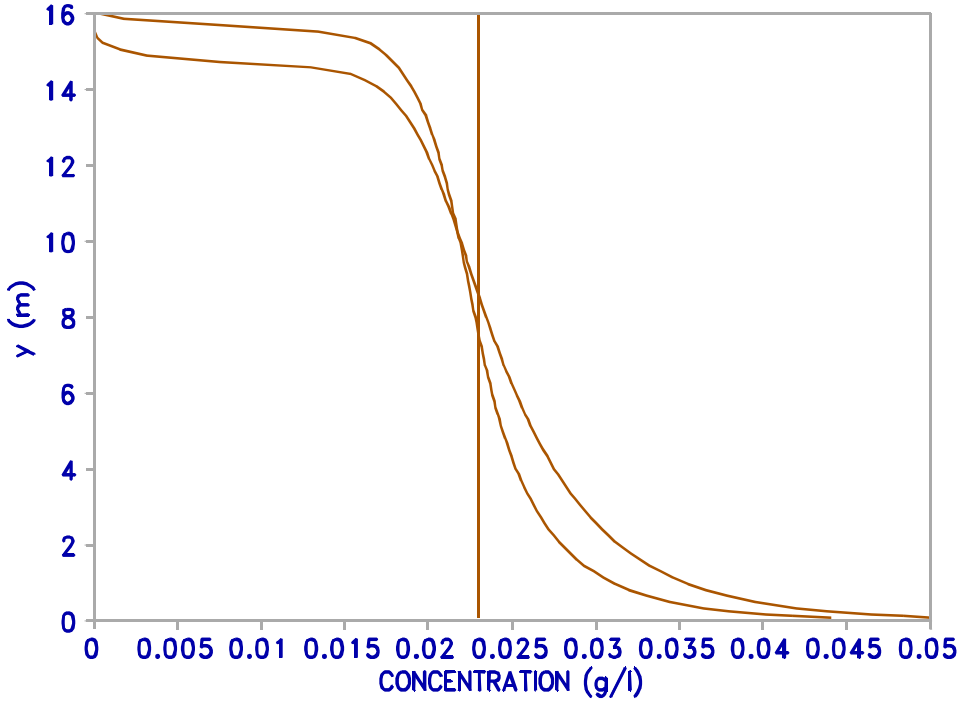


Figure 3.1: Concentration profiles.

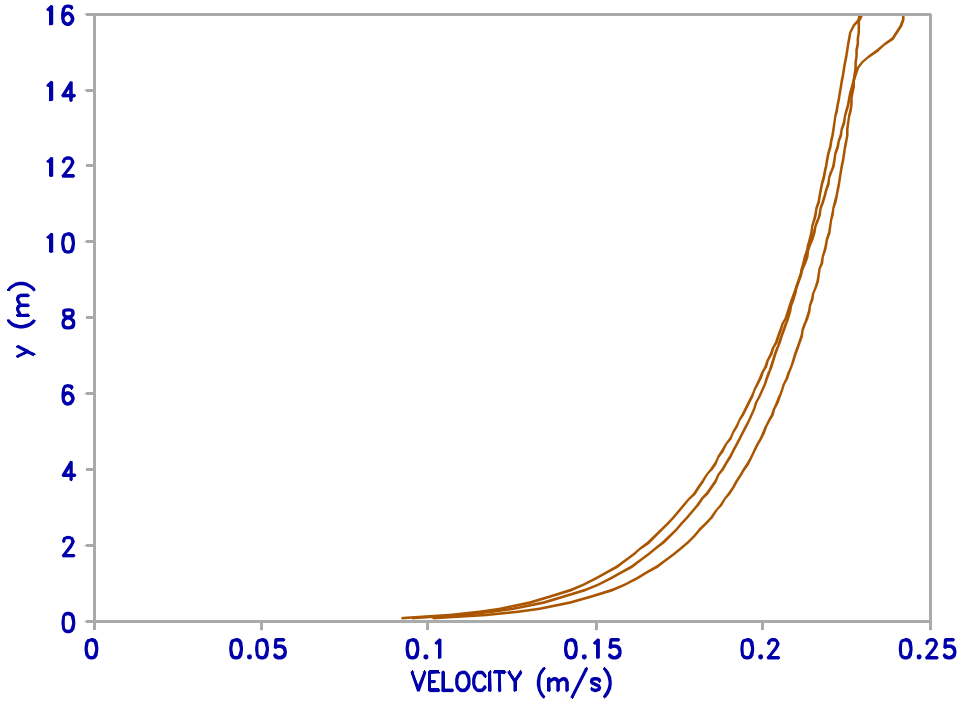


Figure 3.2: Velocity profiles.

$C_0 = 23$ g/l. Results at time $t = 0$, 50 and 100 minutes.

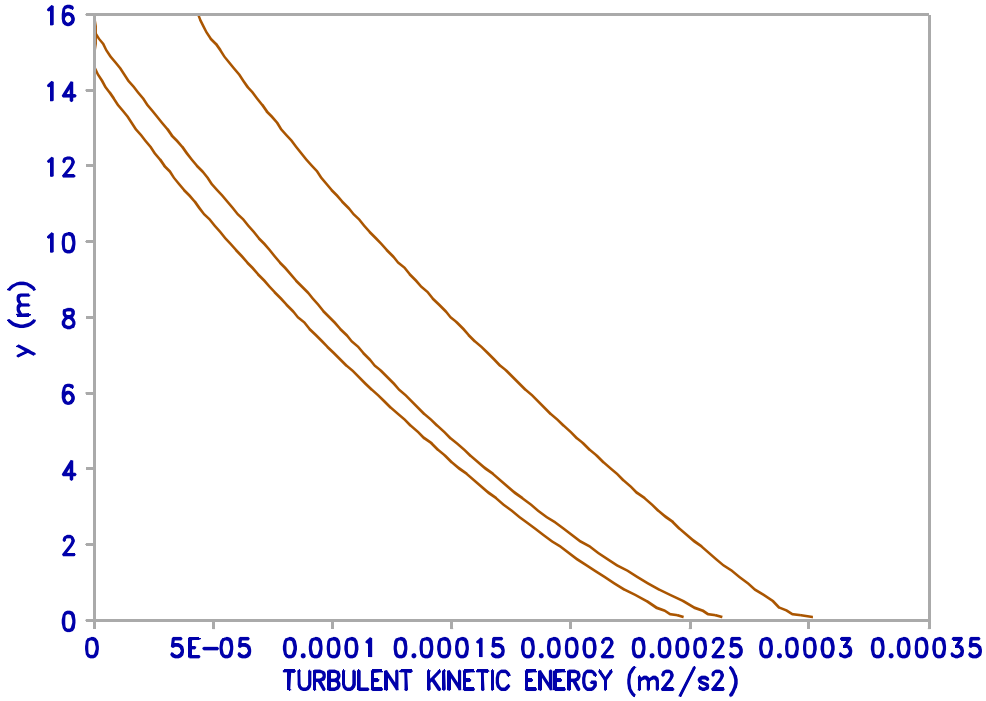


Figure 3.3: Turbulent kinetic energy (k) profiles.

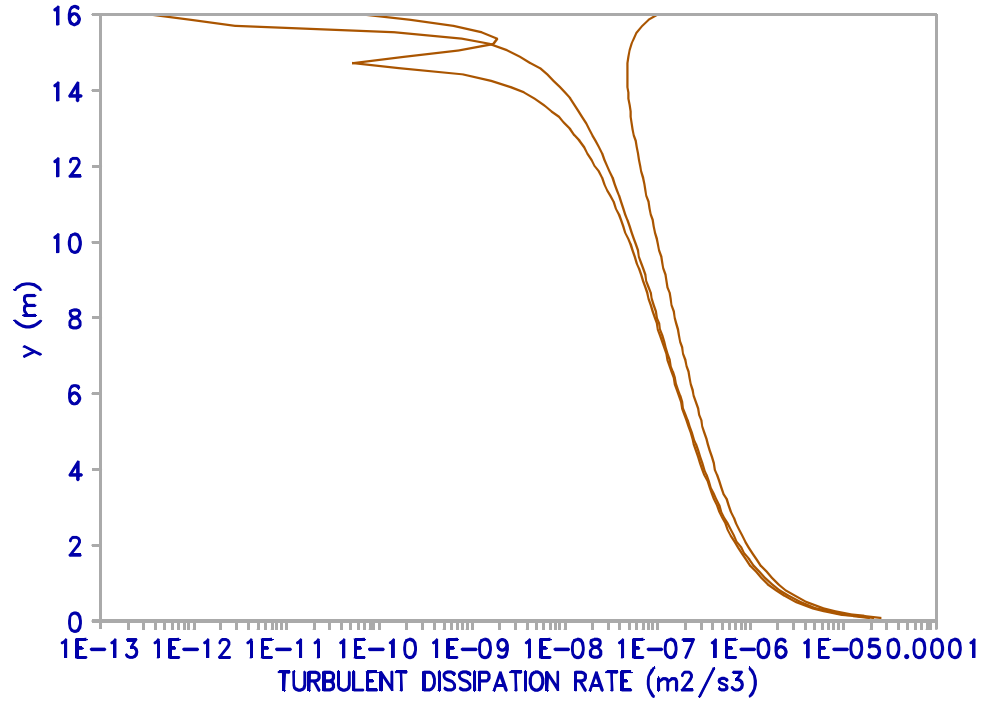


Figure 3.4: Turbulent energy dissipation rate (ε) profiles.

C_0 = 23 g/l. Results at time t = 0, 50 and 100 minutes.

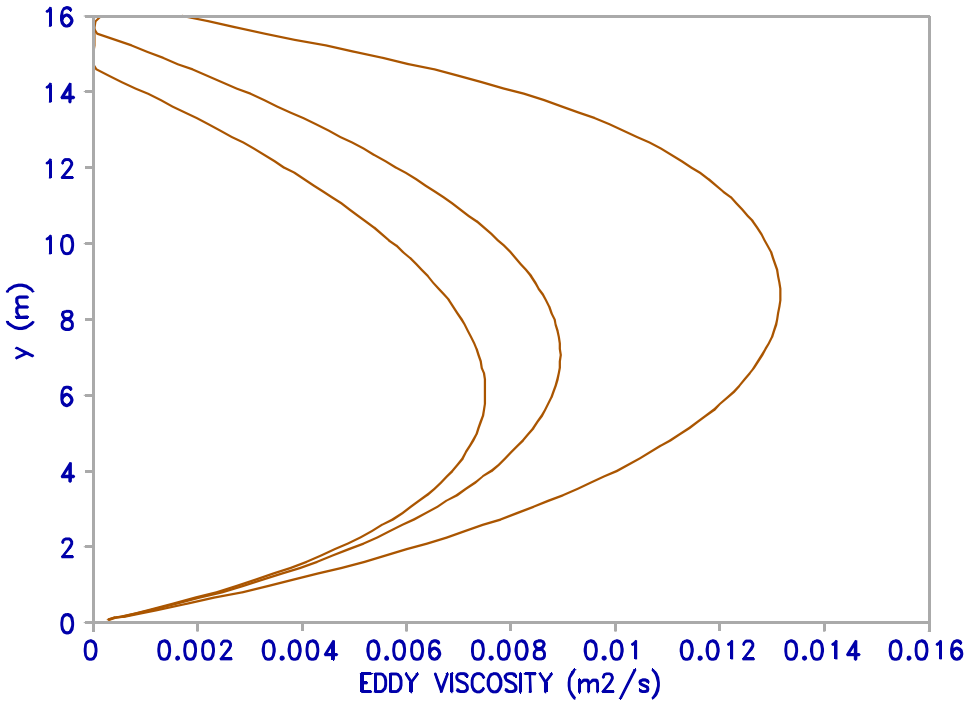


Figure 3.5: Eddy viscosity ($\nu_t = c_\mu k^2/\varepsilon$) profiles.

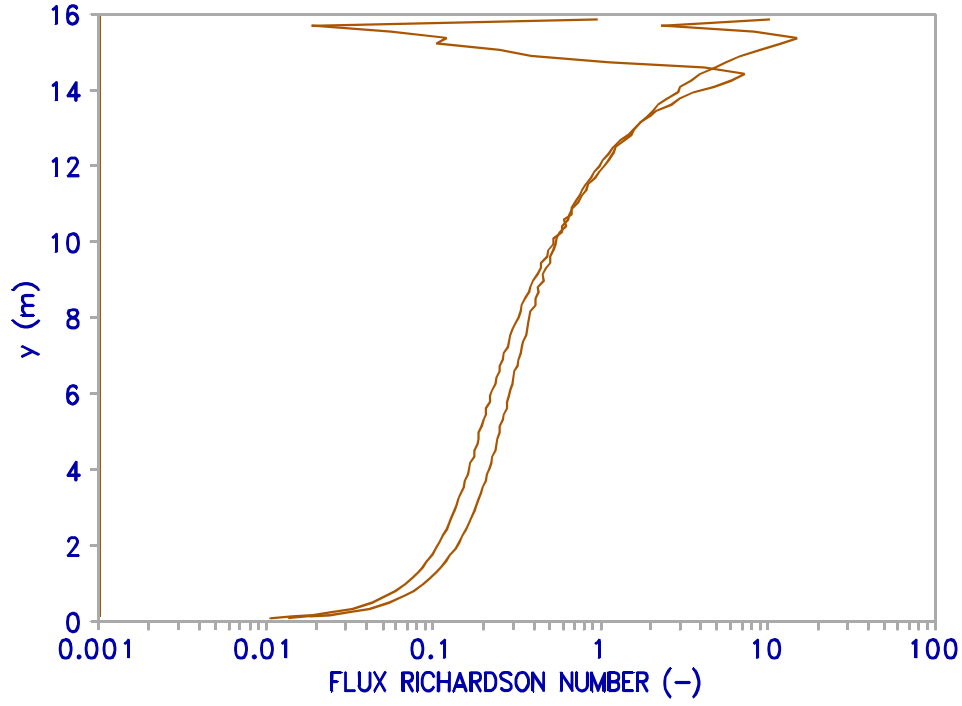


Figure 3.6: Flux Richardson number (*Rf*) profiles.

C_0 = 23 g/l. Results at time t = 0, 50 and 100 minutes.

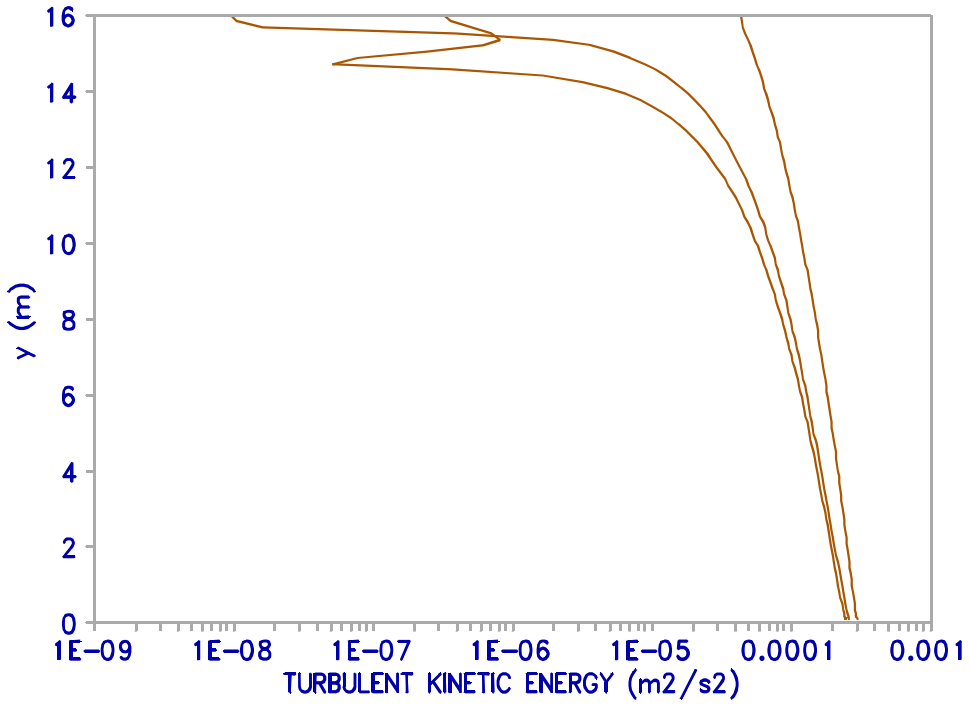


Figure 3.7: Turbulent kinetic energy profiles on semi-log scale.

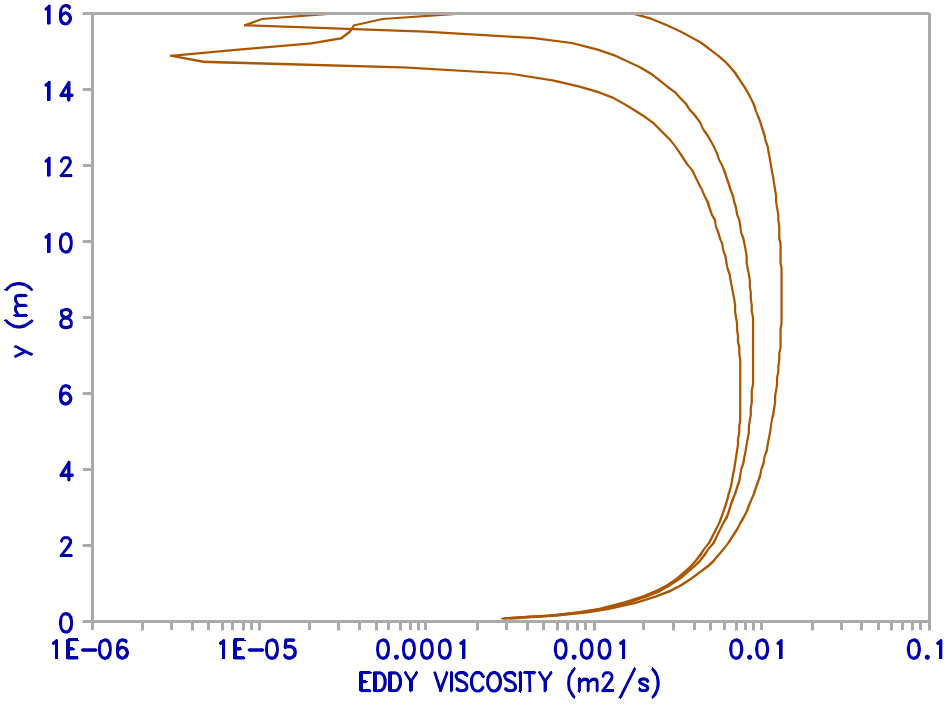


Figure 3.8: Eddy viscosity profiles on semi-log scale.

C_0 = 23 g/l. Results at time t = 0, 50 and 100 minutes.

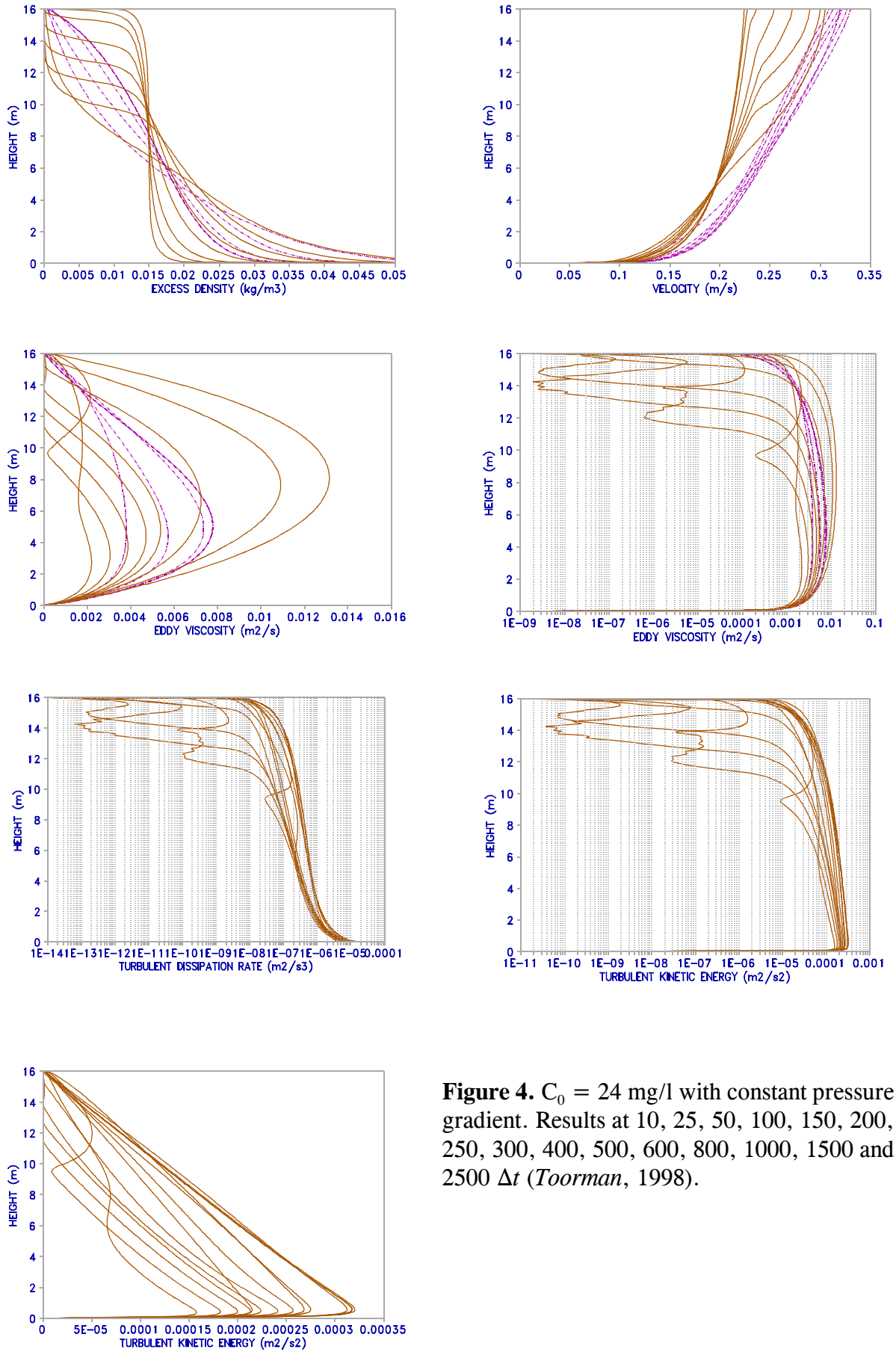


Figure 4. C_0 = 24 mg/l with constant pressure gradient. Results at 10, 25, 50, 100, 150, 200, 250, 300, 400, 500, 600, 800, 1000, 1500 and 2500 Δt (*Toorman*, 1998).

3.10. Numerical diffusion

The results published by *Winterwerp* (1998) do not show the same numerical problems. The minimal values of k and ε obtained by the DELFT-1P model never fall below the critical value for which the FENST-2D model starts having numerical problems. This strongly suggests that the two models differ in the amount of numerical diffusion implicitly generated by the employed numerical scheme.

In order to evaluate the numerical diffusion, a simple test case of sedimentation, derived from the sediment transport model test proposed by *Malcherek* (1995), as suggested and performed by *Uittenbogaard et al.* (1996), has been carried out. The results obtained with FENST-2D are shown in Appendix A. These results, compared to those published by *Uittenbogaard et al.* (1996), confirm that FENST-2D has much less intrinsic numerical diffusion. Consequently, the solutions by FENST are mathematically more accurate. This implies that the numerical problems caused by the excessive damping of turbulence around lutoclines are generated by the fact that the total diffusion (physical + numerical) becomes too small to allow a stable solution of the non-linear turbulence equations.

One could try to resolve the problem by adding artificial diffusion. Several attempts with limited success have been performed. These attempts consist of adding diffusion only there where the eddy diffusion becomes too small. This is done by adding artificial diffusion which is inversely proportional to k.

Another option to be considered is the fact that it is generally known that the eddy viscosity is underestimated in strongly stratified conditions as the buoyancy effect exaggerates the real damping. The physical reason should be sought in the fact that the interface between to fluids becomes unstable as soon as the flux Richardson number falls below the critical value of 0.15. The internal waves generate mixing and thus increase diffusion, which is not accounted for in the present version of the model.

It is concluded from this test case that the standard k-ε turbulence model is unable to handle the damping of turbulence by strong buoyancy effects as it cannot cope with the laminarized region which are created. Consequently, one should modify the k-ε model by implementing damping functions as in low-Reynolds turbulence models. A major problem here is the lack of suitable data to verify the modified models. It is suggested to test first the transition from laminar to turbulent flow and/or vice versa of a clear fluid in simple configuration (e.g. pipe flow), for which some data is available.

4. STEADY STATE CALCULATIONS

Finally, another approach has been adopted. It was found that steady state calculations could be performed when starting with a Rouse-like concentration profile, using pseudo-time stepping for the k-ε equations and the $\Delta\rho$ equation with pseudo-time steps of 120 and 600 seconds respectively. The big advantage is the large gain in computation time.

For each case the pressure gradient ($p' = \mathrm{d}p/\mathrm{d}x$) was kept constant, which is equivalent with a fixed shear velocity, as $u_* = (hp'/\rho)^{1/2}$. Calculations have been performed for various mean concentrations (C_m = 20, 30, 40 and 50 mg/l) and pressure gradients (p' = 0.050, 0.045, 0.040, 0.035, 0.030, 0.025, 0.020, 0.015, 0.012, 0.011, 0.010 and 0.0085 Pa/m, if possible). Typical resulting profiles for C_m = 30 mg/l are presented in figures 5.1-5.6.

4.1. Discussion of *Rf* profiles

Analysis of the results reveals several very interesting facts. The most striking observation is the tendency of *Rf* to become constant over the entire water column (fig.5.4). Deviation at the free surface is caused by the boundary condition (see Section 3.8). At the bottom ($y = \delta$) it is noticed that with decreasing u_*, the growth of *Rf* accelerates. When *Rf* ($y=\delta$) exceeds the constant value, a small decrease of u_* gives already such a large rise of the *Rf* ($y=\delta$) that rapidly the critical value of 1 is exceeded. Physically, $Rf = 1$ means that the production of k is destroyed by buoyancy, i.e. turbulence cannot be generated. This is exactly what explains why the numerical k-ε model fails to converge as the equations are no longer valid. This indicates that some sort of low-*Re* modelling is required around and beyond this point.

A constant value of *Rf* implies $\mathrm{d}Rf/\mathrm{d}y = 0$. This can also be written as:

$$\frac{\mathrm{d}G}{\mathrm{d}y} = -Rf\frac{\mathrm{d}P}{\mathrm{d}y} \qquad \textbf{(21)}$$

Hence:

$$g\ \frac{\mathrm{d}}{\mathrm{d}y}\left(w_s\frac{\Delta\rho}{\rho}\right) = -Rf\,u_*^2\ \frac{\mathrm{d}}{\mathrm{d}y}\left((1-y/h)\frac{\mathrm{d}u}{\mathrm{d}y}\right) \qquad \textbf{(22)}$$

When the settling velocity is constant, one finds:

$$w_s\,g\,\frac{\rho_w}{\rho^2}\frac{\mathrm{d}\rho}{\mathrm{d}y} = -Rf\,u_*^2\ \frac{\mathrm{d}}{\mathrm{d}y}\left((1-y/h)\frac{\mathrm{d}u}{\mathrm{d}y}\right) \qquad \textbf{(23)}$$

Hence:

$$\sigma_s w_s\frac{\rho_w}{\rho}\ (1-y/h)\frac{\mathrm{d}u}{\mathrm{d}y} = -\nu_t\ \frac{\mathrm{d}}{\mathrm{d}y}\left((1-y/h)\frac{\mathrm{d}u}{\mathrm{d}y}\right) \qquad \textbf{(24)}$$

If we can assume a logarithmic velocity profile, a constant κ and $\Delta\rho \ll \rho$, one finds:

$$\nu_t = \sigma_s\,w_s\,y\,(1-y/h) \qquad \textbf{(25)}$$

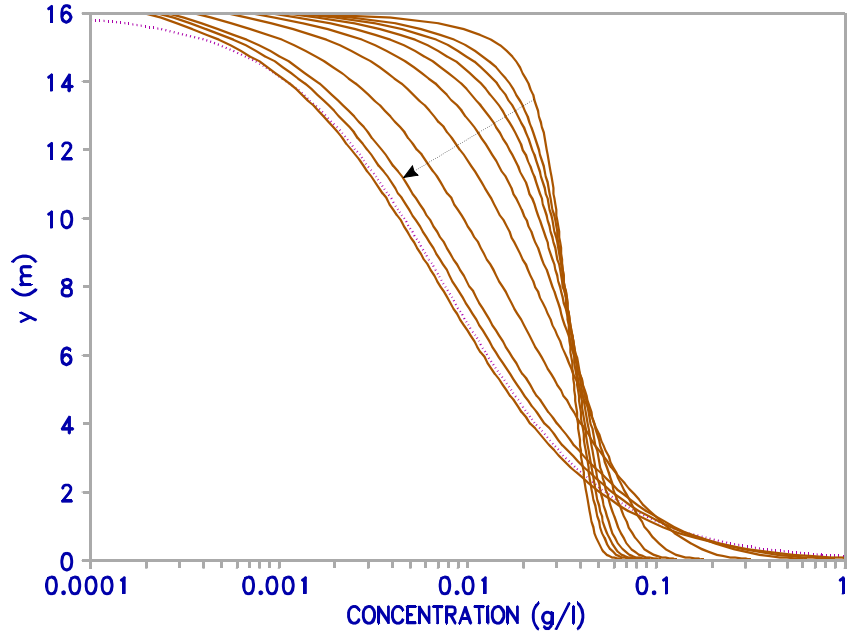


Figure 5.1: Concentration profiles for decreasing u_* (→). Depth-averaged concentration = 30 mg/l. Dotted line = critical Rouse profile (Rouse parameter $Z = \sigma_s w_s/\kappa u_* = 1$).

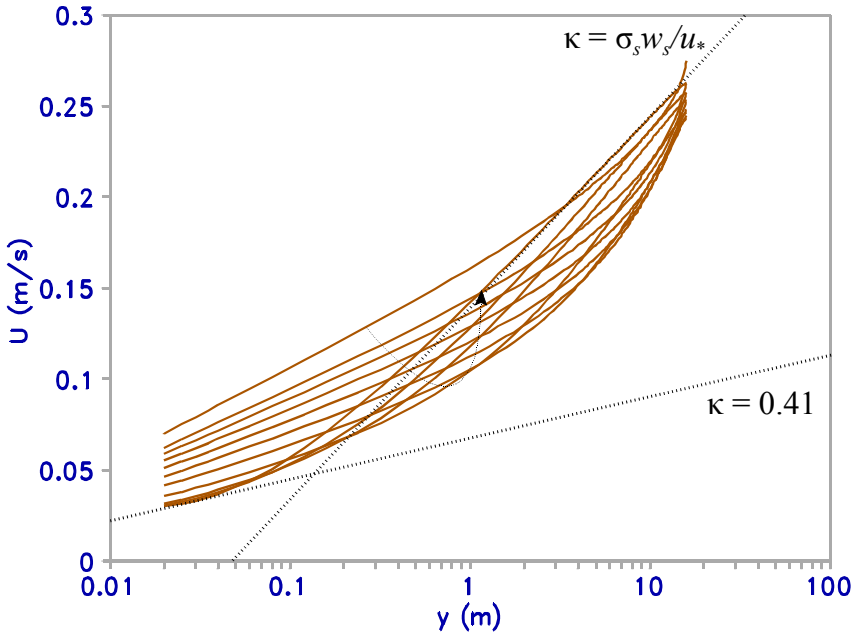


Figure 5.2: Velocity profiles for decreasing u_* (→). Dotted lines = log-laws.

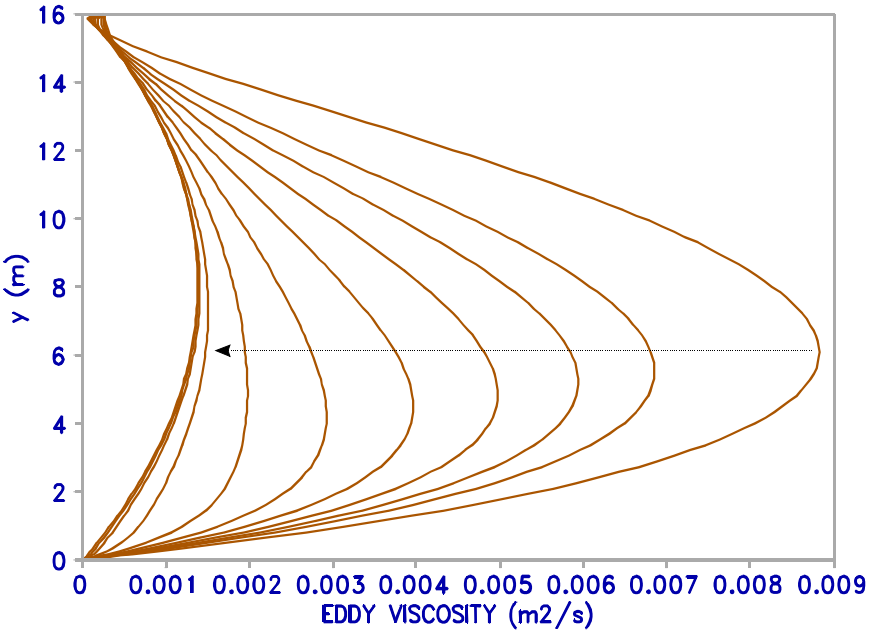


Figure 5.3: Eddy viscosity profiles for decreasing u_* (→).

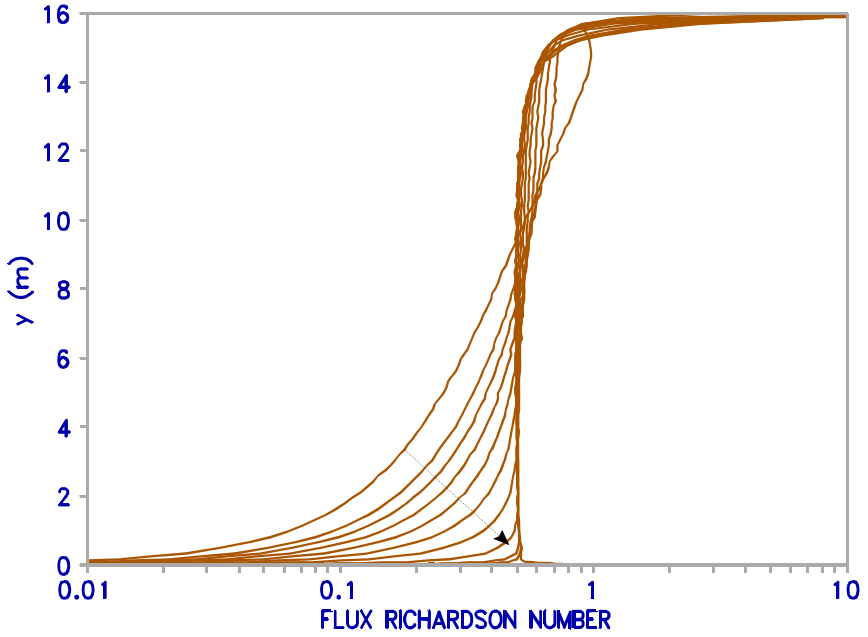


Figure 5.4: Flux Richardson number profiles for decreasing u_* (→).

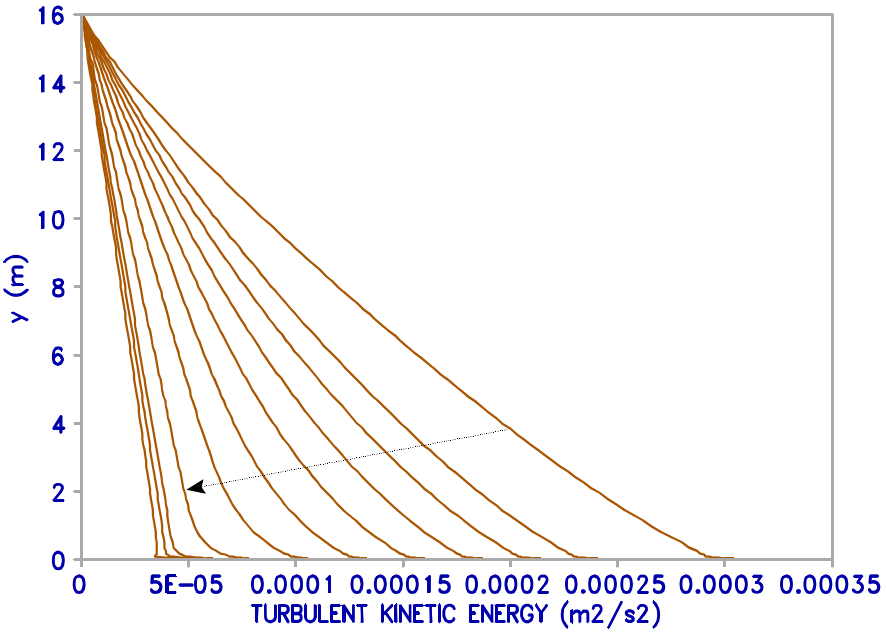


Figure 5.5: Turbulent kinetic energy profiles for decreasing u_* (→).

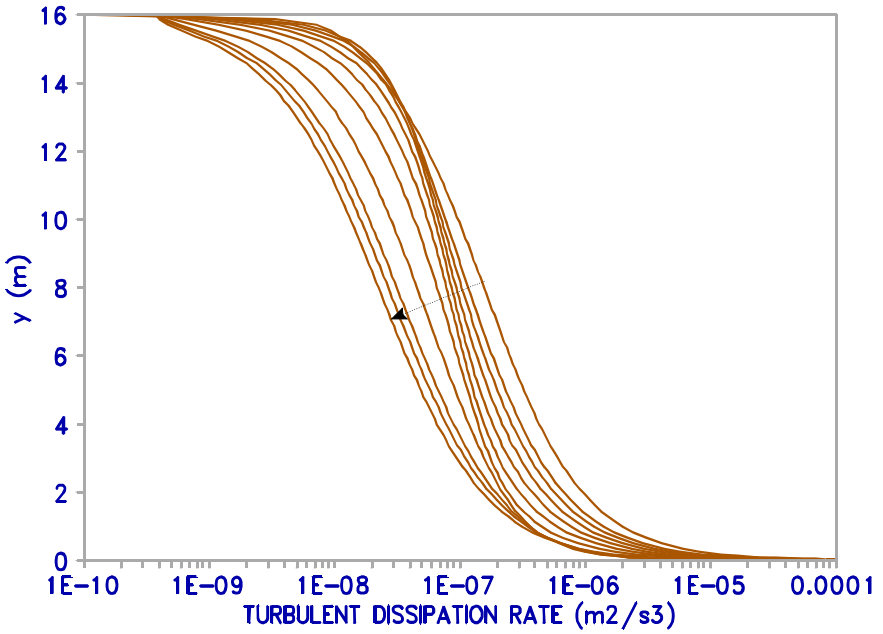


Figure 5.6: Turbulent energy dissipation rate profiles for decreasing u_* (→).

This implies a parabolic eddy viscosity profile.

Notice that the shear velocity does not occur in eq.(25); instead, κu_* is replaced by $\sigma_s w_s$. This theoretical result is confirmed by the numerical results (fig.5.3). When Rf is a constant, then the k-equation is equivalent to a k-equation without buoyancy, but with a production reduced by a constant factor $(1-Rf_c)$. This explains the parabolic profile also.

4.2. Critical Rouse profile

This eddy viscosity profile, eq.(25), substituted into the sediment transport equation yields a concentration profile, corresponding to a Rouse-profile with Rouse parameter value $Z = \sigma_s w_s/\kappa u_* = 1$. Comparison with the simulation shows that this critical Rouse profile indeed is "exceeded" when at the bottom Rf exceeds the constant value (fig.5.1). This Rouse profile is special in the sense that the concentration gradient at the free surface is zero for $Z > 1$ (while $dC/dy = \infty$ at $y = h$ for $Z < 1$).

4.3. Conditions for "saturation"

The constant value of Rf, therefore, seems to be some sort of critical value Rf_c. When it is exceeded, the gradient of Rf changes sign, i.e. becomes negative, and the point of total turbulence collapse ($Rf = 1$) is rapidly reached. This has an important physical meaning, as Rf is the ratio of buoyancy damping to production of TKE (eq.(1)). Hence, when dRf/dy becomes negative, it implies that the buoyancy damping tends rapidly to overcome production towards the bottom. Is is indeed observed that with only a very small increase of p', Rf exceeds the critical value of 1 above which buoyancy damping is dominant.

Interestingly, the production of k as a function of Rf shows a strong “collapse” when $Rf = Rf_c$, i.e. the data show that $\partial P/\partial Rf = -\infty$ at Rf_c (fig.6.1). The profiles of P (fig.6.2) show that the production keeps decreasing away from the bottom, also in the layer where Rf is (approximately) constant, i.e. the “collapse” happens gradually over the entire layer where Rf is constant. The same is seen for the buoyancy damping (and other parameters).

The critical value Rf_c can be found by replacing $-(\nu_t/\sigma_s)d\rho/dy$ by $w_s\Delta\rho$ (equilibrium condition for the mass balance), du/dy by $u_*^2(1-y/h)/\nu_t$ (shear stress distribution) and ν_t by eq.(25) in eq.(1), resulting in:

$$Rf_c = \frac{\sigma_s w_s^2 g}{\rho u_*^4} \frac{y\Delta\rho}{1-\frac{y}{h}} \qquad \textbf{(26)}$$

An approximation is found by substitution of the critical Rouse concentration profile:

$$Rf_c \cong \frac{\sigma_s w_s^2 g}{\rho_w u_*^4} \frac{a\Delta\rho_a}{1-\frac{a}{h}} \qquad \textbf{(27)}$$

The error between the critical Rouse profile and the actual profile is smallest at $y = h/2$.

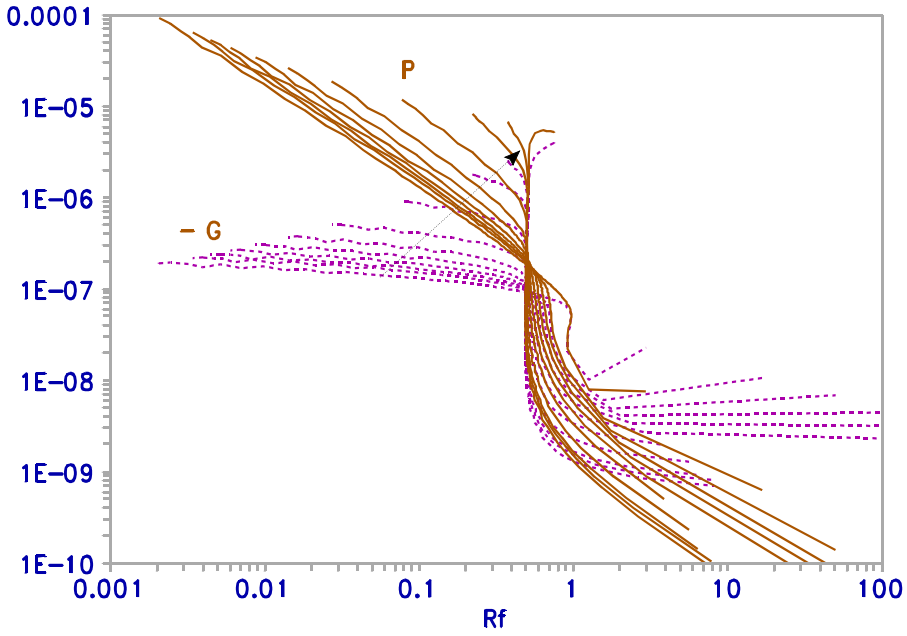


Figure 6.1: TKE production (*P*) and buoyancy damping (-*G*) as a function of *Rf* (*C* = 30 mg/l, δ = 0.02 m, → decreasing u_*)

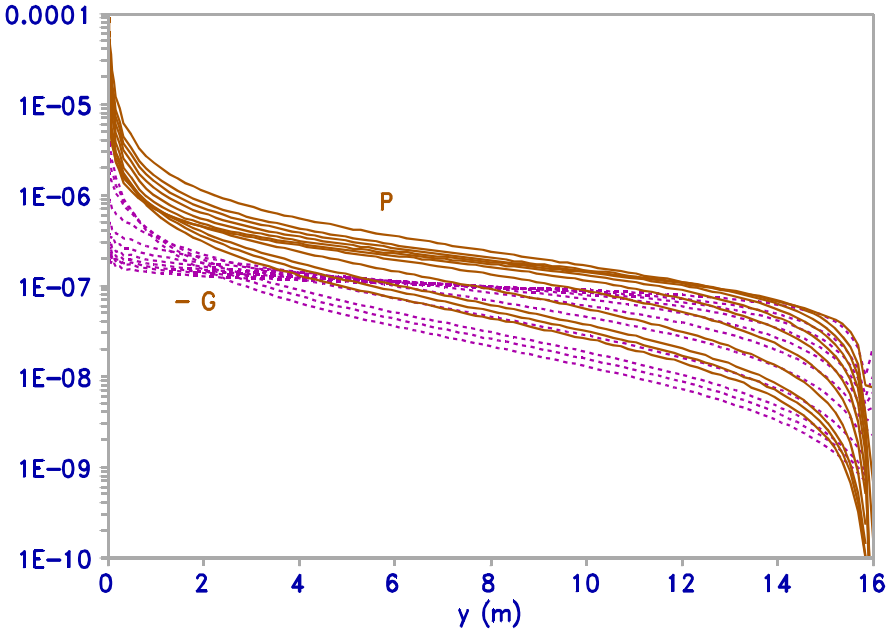


Figure 6.2: Profiles of TKE production (*P*) and buoyancy damping (-*G*), corresponding with fig.6.1.

Therefore, one can use the approximation:

$$Rf_c \cong \frac{\sigma_s w_s^2 g}{\rho_w u_*^4} h\Delta\rho_{h/2} \qquad \textbf{(28)}$$

The value of Rf_c is considerably higher ($Rf_c \approx 0.5$ for the present case where $w_s = 0.5$ mm/s) than the critical value of 0.15 reported in the literature[3]. The numerical tests where w_s and H are held constant show no (or hardly any) variation of Rf_c with u_*, C_m or σ_s. Numerical simulations with other values of w_s indicate that Rf_c decreases slightly and linearly with increasing settling velocity (e.g. $Rf_c \approx 0.45$ for $w_s = 2$ mm/s). Looking at eq.(28), this can be explained by compensation of the increase of w_s by a serious decrease of the concentration in the reference point. The value will be discussed in further depth in section 5.3.

However, as discussed in section 2, no collapse occurs near the surface where Rf can reach values far beyond 1 and even reaches ∞ at the surface itself. Therefore, there should be either another or a second condition which governs collapse. As Rf_c is not a unique value, it seems that the condition for collapse is:

$$\frac{\partial Rf}{\partial y} < 0 \qquad \textbf{(29)}$$

Remarks: (1) For Rouse profiles the gradient of Rf is positive when $Z < 1$ and negative when $Z > 1$ negative. (2) The condition (29) often occurs in a layer where $\partial\nu_t/\partial y > 0$, also for lutoclines (see figs.3.6 and 3.8).

4.4. Saturation concentration

Now that the critical condition can be related to a constant Rf over the water column, it does make sens to integrate of eq.(10) over the water column to calculate the amount of sediment which can be held in suspension. Only, the von Karman constant in (10) has to be replaced by $\sigma_s w_s/u_*$. Hence, the saturation concentration becomes:

$$C_{sat} = \frac{\rho_w u_*^4 Rf_c}{\sigma_s w_s^2 g h \Delta\rho_s/\rho_s} \int_\delta^h \left(\frac{h}{y} - 1\right) dy = \frac{\rho_w u_*^4 Rf_c}{\sigma_s w_s g h \Delta\rho_s/\rho_s} \left(\ln\frac{h}{\delta} + \frac{\delta}{h} - 1\right) \qquad \textbf{(30)}$$

This yields a proportionality with u_*^4 (not exponent 3 as in eq.(10)), which seems to be confirmed by the numerical experiments (fig.7). Eq.(30) does not yield the correct value of the saturation concentration because Rf is not constant near the surface (at least in the present numerical experiments) and because the true concentration profile deviates from the critical Rouse profile at the top and, much more importantly, at the bottom.

[3] The numerical results of *Winterwerp* (1998) yield a value of $Rf_c \approx 0.2$. The difference seems to be related to the effect of numerical diffusion on the results (*cf.* section 3.10).

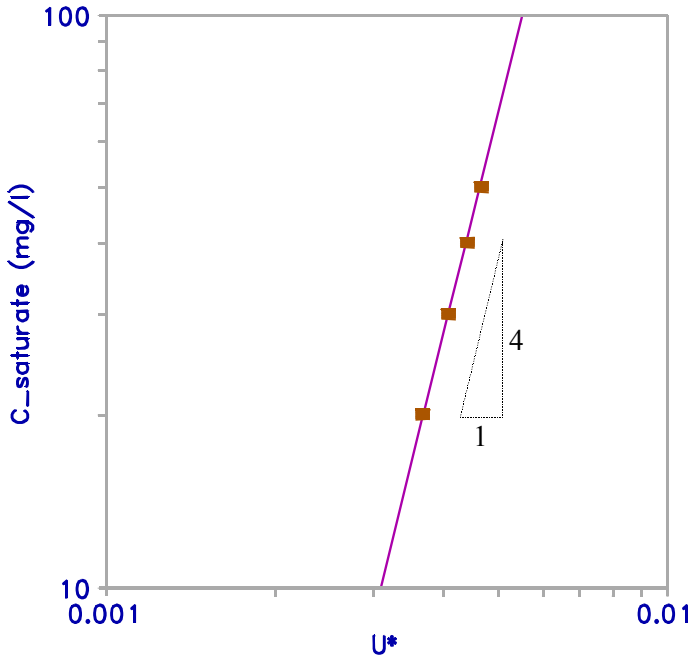


Figure 7: Saturation concentration versus shear velocity ($\delta = 0.02$ m).

4.5. Velocity profile versus the log-law

Elimination of ν_t between eqs.(24) and (25), assuming $\Delta\rho \ll \rho$, yields :

$$\frac{1}{y}\frac{du}{dy} = -\frac{d}{dy}\left((1-y/h)\frac{du}{dy}\right) \qquad \textbf{(31)}$$

Substitution in eq.(23) and elimination of *Rf* with its definition, eq.(1), yields:

$$\frac{du}{dy} = \frac{u_*^2}{\sigma_s w_s y} \qquad \textbf{(32)}$$

This indicates a velocity profile where κ has become equal to $\sigma_s w_s/u_*$. Indeed, the slope of the log-law changes dramatically when the critical condition is approached (fig.5.2). The change of the slope can directly be calculated from the condition $Z = 1$, i.e. κ changes from the von Karman constant to a value $\sigma_s w_s/u_*$. Hence, the log-law changes from:

$$u = \frac{u_*}{\kappa}\ln(y/y_0) \qquad \textbf{(33)}$$

at the bottom (imposed by the boundary condition) to:

$$u = \frac{u_*^2}{\sigma_s w_s}\ln(y/y_1) \qquad \textbf{(34)}$$

away from the bottom (fig.5.2). The value of the roughness parameter y_1 is found to have increased (to 49 mm in the case of fig.5.2).

The difference between bottom and the main stream increases the doubt on the validity of the traditional boundary conditions for k and ε at the bottom for sediment-laden turbulent flows, which are based on the assumption of a constant κ. Experimental data are required to find how the velocity profile changes near the bottom. This, however, seems to be very difficult with the current measurement techniques.

4.6. Distribution of k and ε

The ε distribution can be approximated by the balance $\varepsilon = P+G$. Away from the critical state, the ε profile is hardly affected by the presence of sediment, as no buoyancy term is included in the ε-equation. Assuming a parabolic eddy viscosity profile and a logarithmic velocity profile, one finds:

$$\varepsilon = \frac{u_*^3}{\kappa}\left(\frac{1}{y}-\frac{1}{h}\right)(1-Rf) \qquad \textbf{(35)}$$

Combining this equation with the parabolic eddy viscosity profile for clear water and the relationship $\nu_t = c_\mu k^2/\varepsilon$ yields a linear variation of k.

When the "critical" state is reached, the von Karman coefficient should be replaced by $\sigma_s w_s/u_*$. Hence, the dissipation rate profile can be approximated by:

$$\varepsilon = \frac{u_*^4}{\sigma_s w_s}\left(\frac{1}{y}-\frac{1}{h}\right)(1-Rf_c) \qquad \textbf{(36)}$$

and the k-profile by:

$$k = \frac{u_*^2}{\sqrt{c_\mu}}(1-y/h)\sqrt{1-Rf_c} \qquad \textbf{(37)}$$

The numerical results indeed correspond with these equations, with some deviation near the bottom and the surface (figs. 5.5 and 5.6).

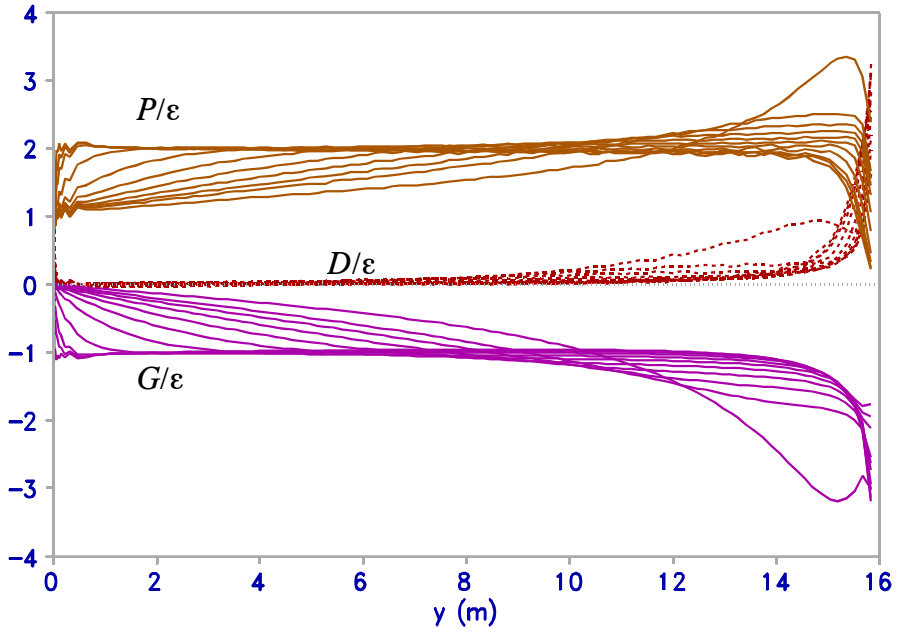


Figure 8.1: Profiles of relative production (P/ε), buoyancy damping (G/ε) and diffusion (D/ε) of turbulent kinetic energy (k) for decreasing u_*.

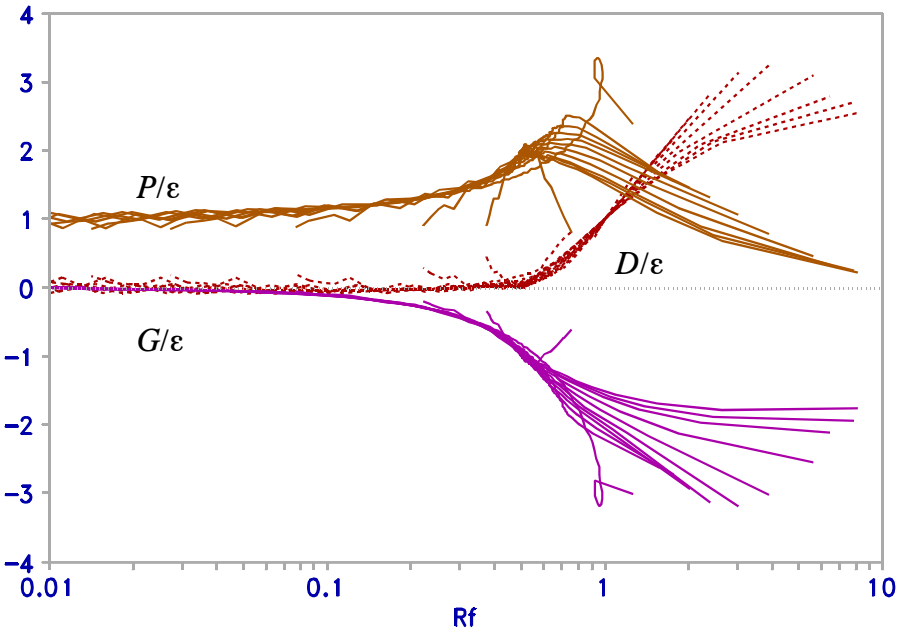


Figure 8.2: Relative production (P/ε), buoyancy damping (G/ε) and diffusion (D/ε) of turbulent kinetic energy (k) as a function of Rf for decreasing u_*.

The diffusion of k around the critical condition ($Rf \approx Rf_c$) can then be calculated:

$$\frac{\partial}{\partial y}\left(\nu_t \frac{\partial k}{\partial y}\right) = \frac{\partial \nu_t}{\partial y}\frac{\partial k}{\partial y} + \nu_t \frac{\partial^2 k}{\partial y^2}$$

$$= \left(\frac{\sigma_s w_s (1-2y/h)}{y}\right)\left(\frac{u_*}{h}\sqrt{\frac{1-Rf}{c_\mu}}\left(\frac{h-y}{2(1-Rf)}\frac{\partial Rf}{\partial y} - 1\right)\right) + O(0) \qquad \textbf{(38)}$$

This shows that the diffusion is always negative, i.e. destabilizes, in the lower half of the water column ($y < h/2$) when $dRf/dy < 0$, or, more general, when $dRf/dy < 2(1-Rf_c)/(h-y)$. Analysis of the numerical data shows that the diffusion is negative over a large part of the water column near the bed, but always very small compared to the production P. However, near the bottom ($y < 0.1$ m), the second term is no longer negligible and even makes the diffusion positive, reaching a value of the same order of magnitude as P or $-G$. This may explain why a solution is still obtained for $Rf_c < Rf < 1$.

The variation of production (P), buoyancy dissipation (G) and diffusion (D) relative to the dissipation rate (ε) is presented in figures 8.1 and 8.2. Figure 8.1 shows that P/ε and G/ε tend to become constant over the entire water column (except near the free surface) around the critical state, reaching values of $1/Rf_c$ and $(Rf_c-1)/Rf_c$ respectively. Figure 8.2 shows that the dissipation remains very small for $Rf < Rf_c$ and rapidly increases (approximately proportional with $\ln Rf$) for $Rf > Rf_c$, providing stability to maintain turbulence.

4.7. Depth-averaged flow velocity

The depth-averaged or mean flow velocity (U) decreases with decreasing u_* down to a minimum, after which its increases again (fig.9). This is explained by the fact that the shear velocity keeps decreasing and, consequently, the bottom friction reduces such that the flow can "accelerate" again. Consequently, turbulent flow over the entire water column with a mean velocity lower that the minimal value is impossible.

As a consequence of this minimum, there is not a unique solution to the "Siltman" test case where U is imposed. Figure 9 shows that two solutions are possible. This explains, at least partially, why the unsteady state simulation of the "Siltman" test case does not always yield the same result as *Winterwerp* (e.g. the results of fig.3 and the results for $C_0 = 30$ mg/l, briefly discussed under the section “Alternative cases”, correspond to the solution on the right side of the minimum).

4.8. Correlations

Analysis of the results suggest a linear correlation between the shear velocity and the corresponding depth-averaged velocity at saturation (fig.9):

$$U_{sat} = A\,u_* - B \qquad \textbf{(39)}$$

For the case with $\delta = 0.02$ m, the parameter values are found to be $A = 84$ and $B = 0.128$. U_{sat} can also be correlated with the depth-averaged excess density as:

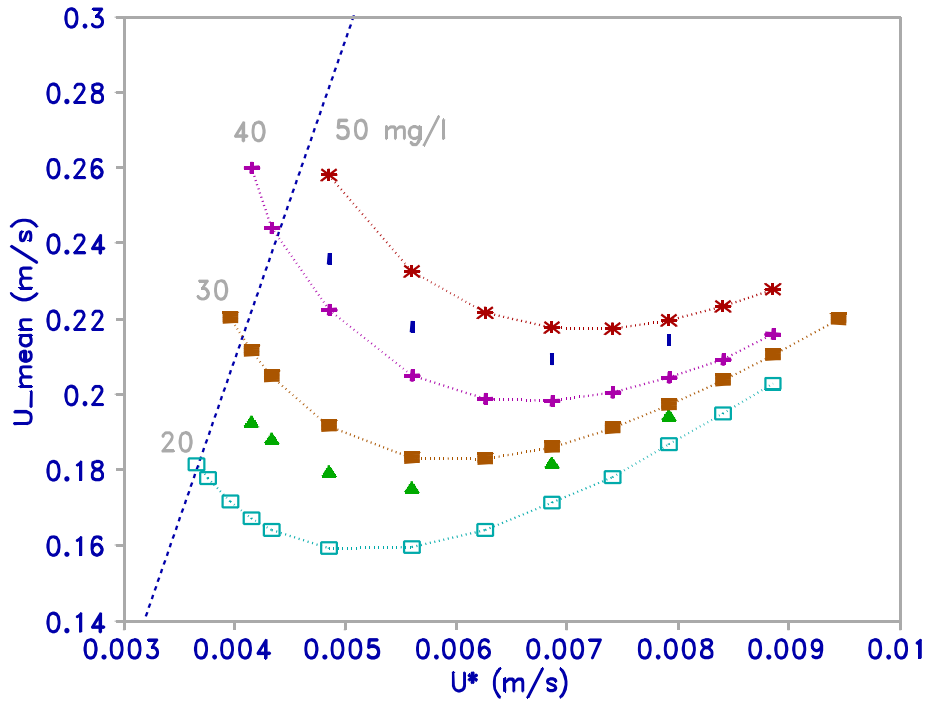


Figure 9: Depth-averaged velocity as a function of shear velocity for steady state conditions ($\delta = 0.02$ m). Dashed line = saturation limit. Unlinked symbols = ▲ 30 and ▌ 50 mg/l with $\delta = 0.08$ m.

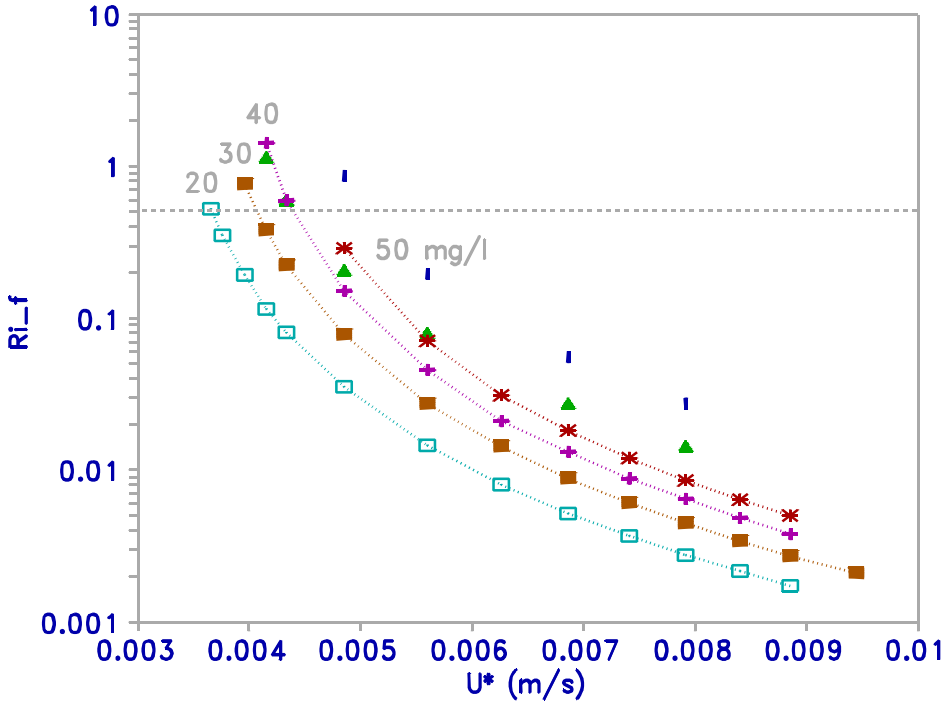


Figure 10: Flux Richardson number in bottom node ($\delta = 0.02$ m) as a function

$$U_{sat} = (C/C_1)^n \qquad \textbf{(40)}$$

of shear velocity for steady state conditions. Dashed line = saturation limit. Unlinked symbols = ▲ 30 and ❙ 50 mg/l with δ = 0.08 m.

For the case with δ = 0.02 m, the parameter values are found to be C_1 = 1300 mg/l and n = 0.41. Based on eq.(40) the saturation concentration for the average velocity of 0.2 m/s of the "Siltman" testcase is found to be 25.65 mg/l, which is slightly more than the value (24 mg/l) found by *Winterwerp* (1998).

Winterwerp (1998) finds a proportionallity between $w_s C_{sat}$ and U to a power 3. The present results suggest a power of ± 2.5.

Extrapolation of the plot of *Rf* at the lowest point (y = δ) as a function of u_* (fig.10) indicates that *Rf* tends to infinity for a certain value of u_*, which will be denoted u_∞. One can fit the all the data with a relationship of the form:

$$Rf(y=\delta) - Rf_{ref} = a\left(u_* - u_\infty\right)^{-n} \qquad \textbf{(41)}$$

with $n \approx 2.8$. A similar relationship holds for p' as $p' \propto u_*^2$.

Remark: The parameter values of the correlations depend on the distance from the wall of the first node, for reasons which are discussed in the next section.

4.9. Wall distance influence

The results are very sensitive to the distance from the wall y = δ of the first node of the computational domain. This is clearly demonstrated in figures 9 and 10. The cause of this non-uniqueness is the bottom boundary condition for the sediment (zero flux, i.e. no sediment exchange with the wall layer is allowed), which forces the sediment to stay within the computational domain. The highest concentration is at the lowest point. However, when this lowest point is further away from the wall, it is found in a layer where the eddy viscosity normally would be higher when buoyancy is neglected. Having the density peak at the higher point will cause here more damping then when the density peak would be lower. Consequently, saturation is reached for higher values of the shear velocity.

Previous discussions suggests that the bottom layer, which contains the viscous sublayer and the transition layer, should be included into the computational domain. This reveals a serious problem of defining a correct bottom distance. The problem is even more complicated because natural sediment bottom are not flat. It is generally assumed that the effective bottom roughness is larger than the thickness of the bottom layer.

4.10. Prandtl mixing length distribution

The steady state results can be used to calculate the corresponding Prandtl mixing length distribution, which is defined by:

$$\ell = \left(\frac{\nu_t}{\frac{\partial U}{\partial y}} \right)^{1/2} \qquad \textbf{(42)}$$

The corresponding ℓ profiles are shown in figure 11.1. The damping function f_ℓ, which corresponds to the buoyancy effect, is then found as:

$$f_\ell = \frac{\ell}{\kappa y\sqrt{1 - y/h}} \qquad \textbf{(43)}$$

This function, for the case $C_m = 30$ mg/l, is shown in figure 11.2. There are two distinct "wings" to the curves, which converge at $Rf = Rf_c$, where the damping function f_ℓ becomes minimal. The minimal value is found by combining equations (25), (32), (42) and (43) to yield $f_{\ell,\min} = \sigma_s w_s/\kappa u_*$. Hence, the damping function is independent on y over the layer where $Rf = Rf_c$. At the same time, when approaching the critical state, the left wing rotates to the right side.

Up to $Rf \approx 0.15$, the damping function can well be approximated by the simple formula:

$$f_\ell \cong 1 - Rf \qquad (Rf < 0.15) \qquad \textbf{(44)}$$

For higher values of Rf the damping function is no longer unique. When the critical condition is approached by decreasing u_*, the left branch of the curve tends to lift and ultimately switches to the right side of the minimum. Above the critical value Rf_c, instead of damping, there seems to be enhanced production. It seems that f_ℓ then asymptotically tends to a proportionallity with Rf (fig.11.2). Notice that $f_\ell\,\kappa$ is equivalent to the corrected von Karman coefficient.

Damping functions proposed in the literature are mostly of the form:

$$f_\ell = (1 + A Rf)^{-n} \qquad \textbf{(45)}$$

For the popular *Munk-Anderson* (1948) formula the parameter values are $A = 10$ and $n = 0.25$. *Kranenburg* (1998) demonstrated that in order to fulfill certain theoretical constraints, the value of the exponent should be $n = 1$. He then finds $A = 2.4$, assuming that the Schmidt number $\sigma_s = 0.7$ (as in the numerical simulation). Comparison with the damping calculated from the k-ε model data shows that neither formula gives a good agreement (fig.11.2).

The plotted relation between f_ℓ and Rf (fig.11.2) shows a striking resemblence with empirical data (fig.12), published by *Monin* (1962), for another correction function f', defined as:

$$\frac{\mathrm{d}u}{\mathrm{d}y} = \frac{u_*}{\kappa L} f'(y/L) \qquad \textbf{(46)}$$

where L = the "Monin-Obukov" length scale, defined as:

$$L = \frac{\rho u_*^3}{\kappa g \overline{\rho' w'}} = -\frac{u_*^3}{\kappa G} \qquad \textbf{(47)}$$

(*Monin & Obukov* (1954) take u_* and the buoyancy flux G as the fundamental parameters to explain the flow properties. All variables then can be expressed as function of y/L, with y the distance from the solid surface). Even though the shape is similar, there are some important differences. The functions are not the same: f' is equivalent to $f_\ell^{-1} y/L$. Secondly, in the data of *Monin*, the minimum corresponds to the critical point for stability of stratification and is reached at the sign reversal of Rf. Finally, the abscise and ordinate in fig.12 are both on a linear scale (logarithmic in fig.11.2). Therefore, the shape resemblance seems to be coincidence.

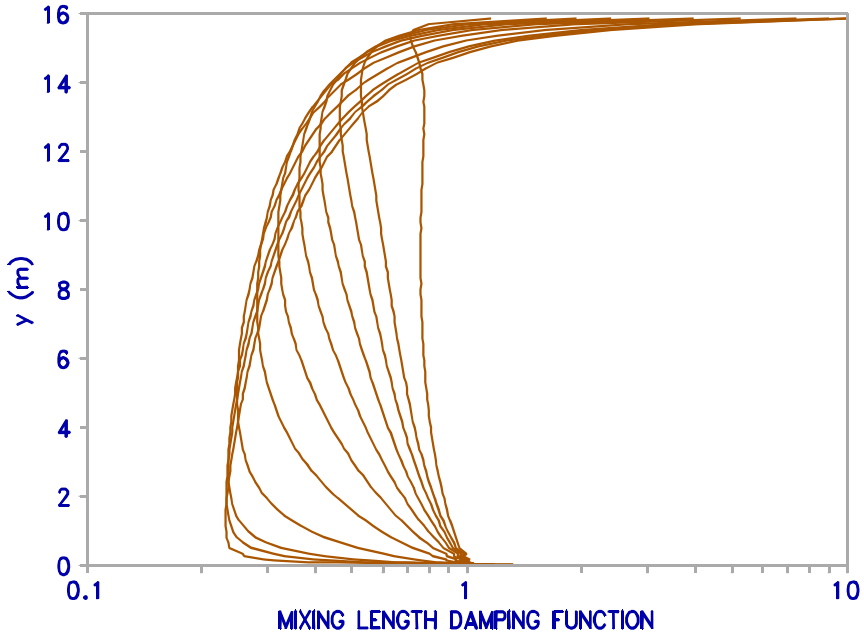


Figure 11.1: Mixing length damping function profiles for decreasing u_* from right to left.

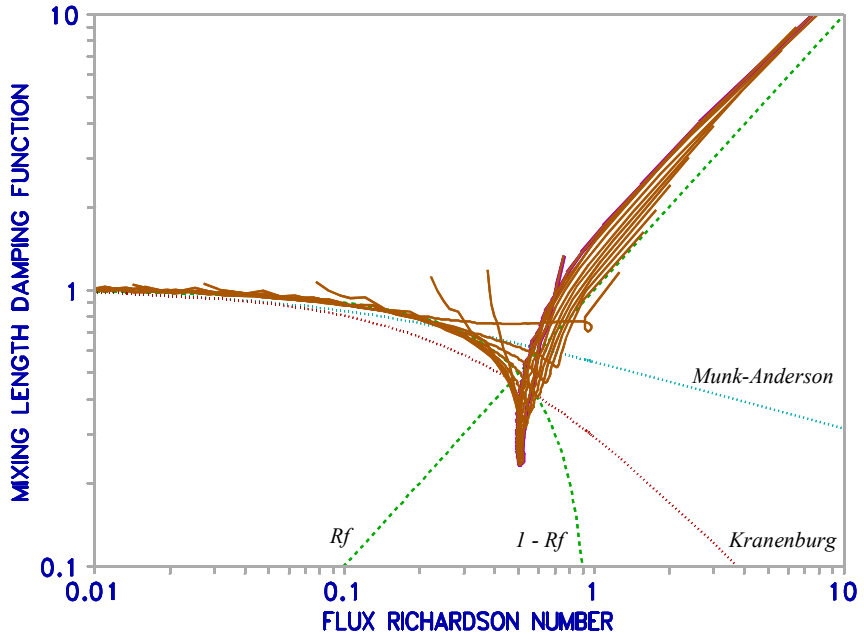


Figure 11.2: Mixing length damping function versus flux Richardson number for decreasing u_*. Dashed lines = 1 - *Rf* and *Rf* respectively. Lower dotted line = *Kranenburg* (1998); uper dotted line = *Munk & Anderson* (1948).

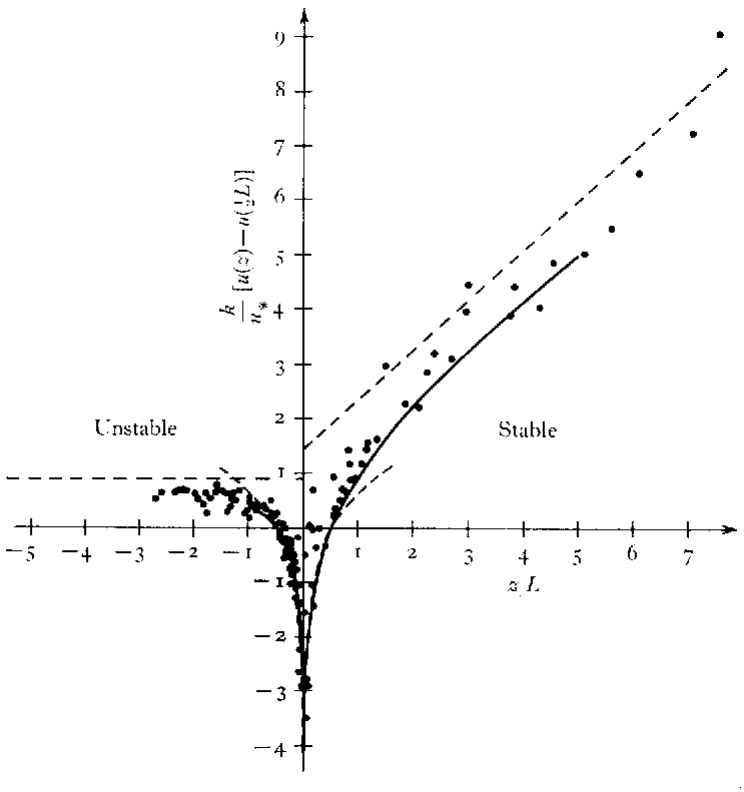


Figure 12: Experimental data of the function $f' = (\kappa L/u_*)\mathrm{d}u/\mathrm{d}z$ as a function of z/L ($= Rf\, u_* z/\nu_t$.; the notation z replaces y, used in the text) in finite difference form (from *Monin*, 1962). The ordinate is equivalent to $f'(z/L) - f'(½)$.

Interesting is the fact that when f' is expressed as a power series in y/L of which the linear term is retained, one finds a log-linear velocity profile:

$$\frac{u}{u_*} = \frac{1}{\kappa}\left(\ln\frac{y}{y_0} + \alpha\frac{y}{L}\right) \qquad \textbf{(48)}$$

with $\alpha \approx 5$ (*Webb*, 1970). Such deviations from the log-law, either stable ($y/L > 0$, i.e. an apparent decrease of κ) or unstable ($y/L < 0$, i.e. an apparent increase of κ), are observed.

5. DISCUSSION & CONCLUSIONS

5.1. Conditions for turbulence collapse

Steady state calculations of fully-developed turbulent, sediment-laden open-channel flow, driven by a constant pressure gradient, indicate that turbulence production collapses when the flux Richardson number Rf exceeds a critical value Rf_c of the order of 0.5, with a relatively weak, linear dependence on the settling velocity. However, the flow retains stability as long as Rf at the bottom remains smaller than the critical value. When $Rf_c < Rf < 1$, a steady state solution can still be found, but the flow has become very sensitive to small variation of the shear velocity. As soon as $Rf > 1$, the solution does no longer converge, because it corresponds to a condition where the turbulence production is completely destroyed by buoyancy damping: as there is no more turbulence generation, the flow should become laminar and the k-ε equations fail as they are no longer valid. The fact of turbulence collapse is nicely illustrated by figure 6.1. It is initiated in the middle of the water column and forms a layer, which thickness increases with decreasing shear velocity.

The critical value of Rf is always exceeded near the surface, without a local collapse of the concentration profile. Collapse of the concentration profile only occurs as soon as the critical value is exceeded at the bottom, which is the source of turbulence production. Hence, a second condition for collapse is $\partial Rf/\partial y < 0$.

5.2. Lutocline formation

The numerical simulations show that a lutocline is generated where $dRf/dz < 0$. The second unsteady test case ($C_0 = 23$ g/l) shows that lutoclines and the associated turbulence collapse can be generated in the upper layer (where the gradient of $\nu_t < 0$), but cannot be maintained (no equilibrium). Lutocline formation can thus also be related to the same stability conditions. Indeed, it can be observed that dRf/dz always turns negative at a lutocline.

5.3. The value of Rf_c

The value of the "critical" flux Richardson number is considerably higher than most empirical data suggest. However, all these empirical data are for density stratification without particles, the majority from thermal stratification or a fresh-salt water combination. Based on the present numerical results, it seems that the critical value in the case of buoyant particles may be higher. Recall that the value of Rf_c is found to depend on the settling velocity, a parameter which is absent in the case of thermal or salt stratification. The settling term in the sediment mas balance equation is a sink term, which probably will alter the stability conditions. As far as known, no stability analysis for particle-laden flows has ever been carried out. There seems to be no dependence on other parameters (except maybe in the case of a Rf-dependent Schmidt number).

Furthermore, it seems that different boundary conditions can play a role (also in stability analysis). These are different in the present case of sediment-laden flow compared to thermal or salt stratification. In thermally stratified flow the temperature is held constant at the upper and lower boundary. In the case of salt-fresh water, stratification cannot be maintained without horizontal salinity gradients.

In the present numerical tests, no mass exchange with the bed is allowed. One may also wonder if in reality, sediment is truly held in suspension when the shear velocity keeps

decreasing. This, of course, depends on the erosion and deposition characteristics, which generally are difficult to determine. But since at equilibrium, the net exchange is zero, the present approach is valid. More questionable is the influence of sediment in the wall-layer which is skipped by the presently used model, imposed by the application of the standard k-ε model. In the present simulation no mass exchange between the wall-layer and the turbulent water column is allowed, which is not realistic, as in reality much sediment may accumulate in this laminar sublayer. However, for practical applications, this re-introduces the problem of how to account properly for the bed roughness. This is a very serious problem that need to looked at more closely in the following research.

As stated in section 2.1, critical values of $Rf < 1$ but > 0.25 cannot be excluded because turbulent kinetic energy still can be available. There are some elementary stratified flows, particularly when vorticity is involved, for which instability occurs at large Rf (*Majda & Shefter*, 1998).

Very recently, experimental data for (non-cohesive) sediment-laden turbulent flow at high concentrations and with measurement of turbulent fluctuations have been published by *Cellino & Graf* (1999). Their data yield values of Rf near the bottom of the order of 0.35-0.55 for their run SLF2 ($Z_{\text{fitted}} = 1.052$) and unrealistically (much) higher values (>1) for the other runs ($1.21 < Z < 1.54$), based on the Rouse profile approximation. The data need to be re-interpreted in the light of the present findings.

5.4. The von Karman coefficient

The theoretical analysis of the condition of a constant Rf leads to analytical profiles for the eddy viscosity, k, ε and velocity u, which correspond to the numerical solution around the critical condition ($Rf = Rf_c$ at the bottom). A major conclusion from this analysis is that the von Karman coefficient changes dramatically to a value of $\kappa = \sigma_s w_s/u_*$, which is considerably smaller than the constant 0.41. It has been known for long from the analysis of experimental concentration profiles in open-channel flows that the von Karman coefficient decreases with increasing sediment load, but it has remained subject of debate, particularly due to the different interpretation of the data by *Coleman* (1986). The present results seem to prove that κ indeed is not a constant. Following the interpretation of eq.(43), it should be replaced by $f_\ell \kappa_K$ (with κ_K the von Karman constant) . This has important implications for the numerical simulation of sediment laden flows. In the case of the standard k-ε model the bottom boundary conditions should be corrected accordingly. The problem then is shifted toward a useful analytical approximation (a parameterization) for the damping function f_ℓ, which seems complicated, as the numerical data indicate that it is not a unique function of Rf.

5.5. The Schmidt number

In the numerical simulations, the Schmidt number σ_s has been held constant and taken equal to 0.7, the value for neutral conditions (no buoyancy), as suggested by *Winterwerp* (1998), based on the work of *Uittenbogaard* (1995). However, experimental data (e.g. figure 1), also show a strong dependency of the Schmidt number on Rf. This can be fitted with empirical damping functions, such as the popular functions of *Munk & Anderson* (1948), or with more theoretically based ones, such as derived by *Ellison* (1957) or *Kranenburg* (1998).

These observations suggest that a varying Schmidt number will affect the value of the critical Richardson number in the numerical simulation and could explain the discrepancy between the value found above and the empirical value of 0.15, which is about three times

smaller. However, this is not the case. Numerical experiments show that the critical value is independent on σ_s, when it is assumed constant. When a damping in function of the gradient Richardson number (*Ri*) is taken into account, like the Munk-Anderson function, the critical Richardson number tends to increase slightly.

Cellino & Graf (1999) have calculated the inverse Schmidt number $\beta = 1/\sigma_s$ for their experiments (their fig.9) which indicate that β decreases with increasing concentration and that β tends towards a linear variation, proportional with y when approaching "capacity" conditions. However, the numerical values are based on the assumption of a constant von Karman coefficient and do not seem realistic (one would expect β to *in*crease with C as Rf then increases). The data will be re-analysed in the follow-up of the present work.

5.6. Degree of saturation

The ratio $<uC>/<u><C>$ (where $<.>$ the depth-averaged value) can be considered as a measure for the transport capacity (TC) of the flow (*Mehta*, 1992). Its value always remains within the limits 0 (no transport) to 1 (homogeneously mixed). *Roberts* (1999) has studied how this ratio evolves when saturation is approached.

Based on this idea, it may be useful to define $s = 1 - TC$ as a measure of the degree of saturation (or stratification), a non-dimensional parameter varying from 0 (no saturation, fully mixed) to 1 (full saturation: all the sediment forms a dense laminar fluid layer at the bottom). Unfortunately, the value of s is very sensitive to the variations of C and u at the bottom, which is very inconvenient when the bottom cannot exactly be defined and when integration is not performed until the bottom. This can also easily be demonstrated with calculating s for a Rouse profile: the value of s is very sensitive to the choice of the near-bottom reference point. For the steady state calculations and the used mesh, the value of s around the critical state is approximately 0.35, which roughly corresponds to the value for a corresponding Rouse profile with $Z = 1$, computed on the same mesh.

5.7. Future work

The present report has revealed some interesting facts on the interaction between suspended sediment and turbulence. At the same time, it has raised many new questions and leaves many of them unanswered. The following subjects will need to be addressed in future research:

- ***Validation***

It should be stressed that the results presented in this report are *numerical* results which have not been verified with experimental data as there are (nearly) no data available which can be used. It is important to realize that assumptions in the numerical model (i.e. a constant von Karman coefficient, a constant Schmidt number, no sediment exchange with the viscous sublayer, constant bottom roughness) do not seem to be realistic at all (not to mention the assumption of isotropic turbulence). Experimental data are required to give further insight. Maybe the recent data of *Cellino & Graf* (1999) can be used, which will be investigated.

Remark: For the simulation of open-channel experiments, it would be better to extend the computational domain to the 2D cross-section of the channel in order to include the influence of secondary currents on the profiles.

• ***Mathematical stability study***

The above analysis of numerical simulation data of fully-developed turbulent sediment-laden open-channel flow suggests that the condition for turbulence collapse is a negative vertical gradient of *Rf*. The ultimate proof should mathematically follow from a stability analysis, in order to see whether conditions with a negative gradient are unstable. This analysis should also yield a corresponding critical flux Richardson number. The analysis should focus on the implications of some fundamental differences with the most studied stratified shear flow cases where no particles are involved: the effect of the additional sink term of the settling term in the particle mass balance equation and the difference in boundary conditions.

The attentive reader may have noticed that the majority of the consulted literature on stability dates from before the 80s. A more up-to-date literature survey need to be carried out. Within that context, several authorities in the field of stratified geophysical flows have been contacted.

•***Transition modelling***

One of the crucial problems in modelling cohesive sediment transport (CST) in an estuarine environment with a two-equation turbulence model is the transition from turbulent to laminar regime and vice versa, which occurs at the reversing of the tides and around lutoclines. A quick inventory learns that the modelling of transitional flows has only been relatively successful for the special case of wall bounded shear flows with adapted low-Reynolds models. These models are too expensive for engineering applications of CST models. This is a major concern which needs prior attention in future research[4].

• ***Bottom interaction***

As explained previously, it will be important to study the influence of inclusion of the thin bottom layer, comprising the laminar sublayer, which is skipped with the traditional k-ε model. It will be interesting to redo the 1D test cases with low-Reynolds models in order to see how the results differ, since they do not use the von Karman coefficient. These models allow sediment exchange with the sublayer, where the concentration can be expected to be the highest, which may become very important around the saturation point, as the contribution of this layer to the total sediment load may no longer be negligible. Unfortunately, it is likely that the damping functions of the low-*Re* models may no longer be valid as they are semi-empirically fitted with data in homogeneous fluids.

Secondly, the problem of the roughness needs to be addressed. Including the wall layer involves including the true roughness indirectly in order to account correctly for the amount of sediment which can be present in this layer. Practically, this is problematic as the roughness heights in estuaries generally are larger than the thickness of the laminar sublayer. A pragmatic solution should be found. Furthermore, the numerical simulations in this report indicate that the apparent roughness may change.

---

[4] Apparently, the DELFT-3D model is able to overcome this problem by using an ingeneous solver (confidential for commercial reasons), which ensures positive values of for the k and ε under all circumstances. However, intercomparison with the research code FENST, used in this report, indicates that the numerical scheme in the Delft code generates a lot of numerical diffusion (*cf.* Section 3.11) and it has not been demonstrated how well the obtained results around transition correspond with reality. As the code is developed for commerical purposes, priority is given to robustness.

Acknowledgements

This work has been carried out within the framework of the MAST III COSINUS project, partially funded by the European Commission, Directorate General XII for Science, Research and Development under contract no. MAS3-CT97-0082.

The author's position as Post-doctoral Researcher has been provided by the *Flemish Fund for Scientific Research*.

Simulation data obtained with the DELFT-1P model were kindly provided by J.C. Winterwerp (*WL|Delft Hydraulics*).

REFERENCES

Booij, R. (1992). *Turbulentie in de Waterloopkunde* (Turbulence in Hydraulics). Course B82 Textbook, Dept. of Civil Engineering, T.U.Delft, 141 pp. (in Dutch).

Businger, J.A. (1969). Note on the critical Richardson number(s). *Quart. J. Roy. Met. Soc.*, 95:653-654.

Chandrasekhar, S. (1961). *Hydrodynamic and Hydromagnetic Stability*. Clarendon Press, Oxford.

Cellino, M. & W.H. Graf (1999). Sediment-laden flow in open channels under noncapacity and capacity conditions. *J. Hydr. Eng.*, 125(5):456-462.

Coleman, N.L. (1986). Effects of suspended sediment on the open channel velocity distribution. *Water Resources Res.*, 22(10):1377-1384.

Drazin, P.G. (1962). On stability of parallel flow of an incompressible fluid of variable density and viscosity. *Proc. Camb. Phil. Soc.*, 58:646-661.

Drazin, P.G. & Howard, L.N. (1966). Hydrodynamic stability of parallel flow of inviscid fluid. *Advanc. Appl. Mech.*, 9:1-89.

Ellison, T.H. (1957). Turbulent transport of heat and momentum from an infinite rough plane. *J. Fluid Mech.*, 2:456-466.

Goldstein, S. (1931). On the stability of superposed streams of fluids of different densities. *Proc. Roy. Soc. A*, 132:524-548.

Howard, L.N. (1961). Note on a paper of John W. Miles. *J. Fluid Mech.*, 10:509-512.

Jacobitz, F.G., S. Sarkar & C.W. Van Atta (1997). Direct numerical simulation of the turbulence evolution in a uniformly sheared and stably stratified flow. *J. Fluid Mech.*, 342:231-261.

Ludman, F.H. (1967). Characteristics of billow clouds and their relationship to clear air turbulence. *Quart. J. Roy. Met. Soc.*, 93:419-435.

Majda, A.J. & M.G. Shefter (1998). Elementary stratified flows with instability at large Richardson number. *J. Fluid Mech.*, 376:319-350.

Malcherek, A. (1995). Mathematische Modellierung von Strömungen und Stofftransport-prozessen in Ästuaren. PhD thesis, Bericht nr. 44/1995, Inst. fur Strömungsmechanik und ERiB, Universität Hannover, 203 pp.

Mehta, A.J. (1992). *Estuarine cohesive sediment transport*. Lecture Notes OCP6297, Coastal & Oceanographic Eng. Dept., University of Florida, Gainesville.

Miles, J.W. (1961). On the stability of heterogeneous shear flows. *J. Fluid Mech.*, 10:496-508.

Monin, A.S. (1962). Empirical data on turbulence in the surface layer of the atmosphere. *J. Geophys. Res.*, 67:3103-3109.

Monin, A.S. & Obukov, A.M. (1954). Basic laws of turbulent mixing in the ground layer of the atmosphere. *Acad. Sci. U.S.S.R. Leningrad Geophys. Inst.*, 24:163-187 (in Russian).

Munk, W.H. & Anderson, E.A. (1948). Notes on a theory of the thermocline. *J. Marine Research*, 3(1):276-295.

Kranenburg, C. (1998). Saturation concentrations of suspended fine sediment. Computations with the Prandtl mixing-length model. Report No.5-98, Hydromechanics Section, Fac. Civil. Engrg. & Geosciences, T.U.Delft, 11 pp. + figs.

Richardson, L.F. (1920). The supply of energy from and to atmospheric eddies. *Proc. Roy. Soc., A*, 97:354-373.

Richardson, L.F. (1925). Turbulence and vertical temperature difference near trees. *Phil. Mag.*, 49:81-90.

Roberts, W. (1999). Personal communication.

Rodi, W. (1980). *Turbulence Models and their Application in Hydraulics*. State-of-the-Art Paper, IAHR, Delft.

Stull, R.B. (1988). *An Introduction to Boundary-Layer Meteorology*. Kluwer Academic Press.

Taylor, G.I. (1931). Effect of variation of density on the stability of superposed streams of fluid. *Proc. Roy. Soc. A*, 132:499-523.

Toorman, E.A. (1998). Modelling lutocline formation in mud-laden turbulent flow. Preliminary results. *COSINUS 1st Annual General Meeting*, Book of Abstracts pp.27-28.

Toorman, E.A. (1999). Sedimentation and self-weight consolidation: constitutive equations and numerical modelling. *Géotechnique*, 49 (in press).

Turner, J.S. (1973). *Buoyancy Effects in Fluids*. Cambridge University Press.

Uittenbogaard, R.E. (1995). The importance of internal waves for mixing in a stratified estuarine tidal flow. PhD thesis, T.U.Delft.

Uittenbogaard, R.E., J.C. Winterwerp, J.H.Th.M. van Kester & H. Leepel (1996). 3D cohesive sediment transport. A preparatory study about implemetation in DELFT3D. *Report Z1022* (Parts 1 & 2), WL|Delft Hydraulics, Delft.

Webb, E.K. (1970). Profile relationships: the log-linear range and the extension to strong stability. *Quart. J. Roy. Met. Soc.*, 96:67-90.

Werne, J. & D.C. Fritts (1999). Stratified shear turbulence: evolution and statistics. *Geophys. Res. Letters*, 26(4):439-442.

Winterwerp, J.C. (1998). SILTMAN: Analysis of field measurements. *Report Z2263*, WL|Delft Hydraulics, Delft.

Winterwerp, J.C. (1999). *On the Dynamics of High-Concentrated Suspensions*. PhD thesis, T.U.Delft.

***Appendix*: Sedimentation with bottom adsorption**

Malcherek (1995) advises to use a test case proposed by *Lavelle et al.* (1981). Consider the general unsteady-state advection-diffusion equation for sediment transport with initial condition:

$$C(z,0) = C_0\, e^{-\gamma z} \tag{A.1}$$

and boundary conditions:

$$\begin{aligned} S(0,t) &= w_s\, C + \nu \frac{\partial C}{\partial z} = \theta\, C(0,t) \\ S(H,t) &= 0 \end{aligned} \tag{A.2}$$

where: S = sediment flux, ν = diffusion coefficient, θ = adsorption rate and γ a constant. A general analytical solution can be obtained in the presence of uniform advection by separation of variables (*Malcherek*, 1995). The test case can be reduced to a 1D case without advection, as done by *Uittenbogaard et al.* (1996). The corresponding analytical solution is given by *Malcherek* (1995) as:

$$\frac{C(z,t)}{C_0} = \frac{1}{2}\, e^{-(2\beta\nu-\gamma)\gamma t} \left[e^{-\gamma t}\, erfc(x_1) + c_1 e^{(\gamma-2\beta)z}\, erfc(x_2) \right] + c_2\, e^{-(2\beta-\theta/\nu)(z+\theta t)}\, erfc(x_3)$$

$$\begin{aligned} c_1 &= \frac{\gamma - 2\beta + \theta/\nu}{\gamma - \theta/\nu} \\ c_2 &= \frac{\gamma - 2\beta + \theta/\nu}{\beta - \theta/\nu - (\beta-\gamma)^2/(\beta-\theta/\nu)} \\ x_1 &= (\gamma-\beta)\sqrt{\nu t} - \frac{z}{2\sqrt{\nu t}} \\ x_2 &= (\gamma-\beta)\sqrt{\nu t} + \frac{z}{2\sqrt{\nu t}} \\ x_3 &= (\theta/\nu-\beta)\sqrt{\nu t} + \frac{z}{2\sqrt{\nu t}} \\ \beta &= w_s/2\nu \end{aligned} \tag{A.3}$$

Numerical results for this 1D case, obtained with the FENST-2D code are compared with the analytical solution in figure B.1. The Fortran program to calculate the analytical solution is given below. The error function is computed with truncation of its series expansion after six terms.

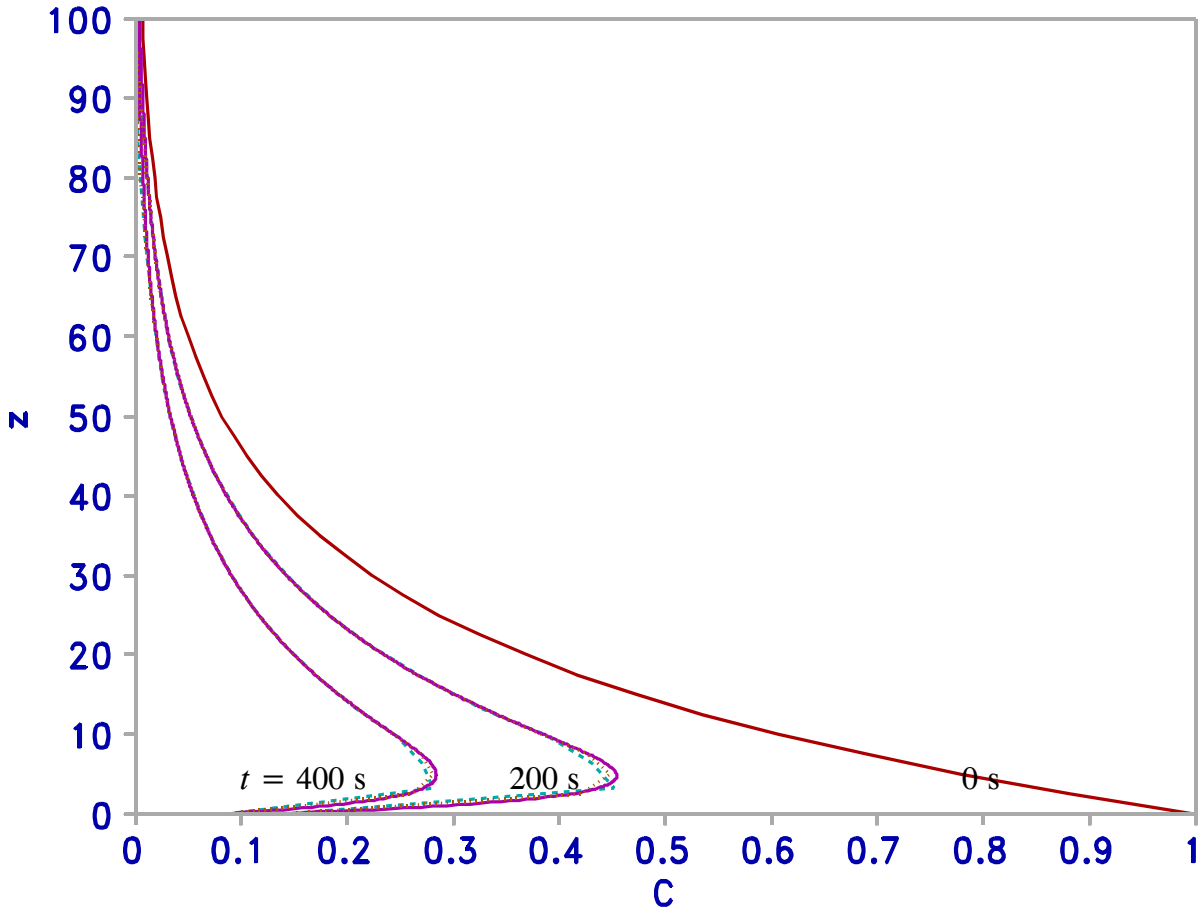


Figure B.1: Finite element simulation (FENST-2D solution) of the Malcherek test case with parameter values: w_s = 0.05 m/s, ν = 0.1 m^2/s, θ = 0.2 m/s, γ = 0.05 m^{-1}. Time step Δt = 1 s. Results[5] at time t = 0, 200 and 400 s. Full line = analytical solution, dashed line = 10 elements (21 nodes) not equally distributed (refinement factor 1.1), dotted line = 20 elements (51 nodes) equally distributed.

REFERENCES

Lavelle, J.W., E. Otzturgut, S.A. Swift & B.H. Erickson (1981). Dispersal and resedimentation of the benthic plume from deep-sea mining operations: a model with calibration. *Marine Mining*, 3:59-93.

Malcherek, A. (1995). Mathematische Modellierung von Strömungen und Stofftransport-prozessen in Ästuaren. PhD thesis, Bericht nr. 44/1995, Inst. fur Strömungsmechanik und ERiB, Universität Hannover, 203 pp.

Uittenbogaard, R.E., J.C. Winterwerp, J.H.Th.M. van Kester & H. Leepel (1996). 3D cohesive sediment transport. A preparatory study about implemetation in DELFT3D. Report Z1022 (Parts 1 & 2), Delft Hydraulics.

[5] The linear interpolation is an artefact of the straight connection of the data points by the spreadsheet software, which cannot account for the quadratic interpolations used by the FE code.

Fortran program to solve eq.(A.3)

```
       PROGRAM SEDTEST1
C=======================================================================
C      Analytical solution for the 1D sedimentation+adsorption test case
C      as defined by Malcherek (1995)
C      with parameter values as Uittenbogaard et al. (1996)
C      Written by Erik A. Toorman
C      (C)1999 Hydraulics Laboratory, K.U.Leuven
C=======================================================================
       implicit double precision(a-h,o-z)

       open(10,file='malch.out',status='old')
       write(*,*)' time ?'
       read (*,*)  time
       H =100.0
       Ws=0.05
       g =0.05
       v =0.1
       t =0.2
       a =Ws/2/v
       d =g-2*a
       e =t/v
       c1=d*g*v*time
       c2=(d+e)/(g-e)
       c3=(d+e)/((a-e)-(a-g)**2/(a-e))
       c4=2*a-e
       c0=sqrt(v*time)

       DO 1 i=1,1001
       y=(i-1)*H/1000
       x1=(g-a)*c0-y/2/c0
       x2=(g-a)*c0+y/2/c0
       x3=(e-a)*c0+y/2/c0
       write(10,1001)erfc(x1),erfc(x2) ,erfc(x3)
       write(10,1001)exp(c1) ,exp(-g*y),exp(-c4*(y+t*time))
       C=exp(c1)*(exp(-g*y)*ERFC(x1)+c2*exp(d*y)*ERFC(x2))/2
     &  -c3*exp(-c4*(y+t*time))*ERFC(x3)
       write(10,1001)y,C
    1  CONTINUE
 1001  format(3(g11.5,1x))
       END
C=======================================================================
       DOUBLE PRECISION FUNCTION ERFC(x)
C      > Error function (truncated after 6 terms)
       implicit double precision(a-h,o-z)
       pi=acos(-1.d0)
       ERFC=2/sqrt(pi)*(x-x**3/3+x**5/10-x**7/42+x**9/216-x**11/1320)
       RETURN
       END
C=======================================================================
```